

EDITORIAL BOARD

Tudor BÎNZAR – Editor in Chief

Liviu CĂDARIU

Executive Editor for Mathematics
liviu.cadariu-brailoiu@upt.ro

Dușan POPOV

Executive Editor for Physics,
dusan.popov@upt.ro

Camelia ARIEȘANU, Department of Mathematics, Politehnica University Timisoara

Nicolae M. AVRAM, Faculty of Physics, West University of Timisoara

Titu BÂNZARU, Department of Mathematics, Politehnica University Timisoara

Nicolae BOJA, Department of Mathematics, Politehnica University Timisoara

Emeric DEUTSCH, Politechnic University-Brooklyn, New York, U.S.A.

Sever S. DRAGOMIR, School of Engineering & Science, Victoria University of Melbourne, Australia

Mirela FETEA, Department of Physics, University of Richmond, U.S.A.

Marian GRECONICI, Depart. of Physical Fundamentals of Engineering, Politehnica University Timisoara

Pașc GĂVRUȚA, Department of Mathematics, Politehnica University Timisoara

Jovo JARIĆ, Faculty of Mathematics, University of Belgrade, Serbia

Maria JIVULESCU, Department of Mathematics, Politehnica University Timisoara

Darko KAPOR, Institute of Physics, University of Novi Sad, Serbia

Octavian LIPOVAN, Department of Mathematics, Politehnica University Timisoara

Dragoljub Lj. MIRJANIĆ, Academy of Science and Art of the Republic of Srpska, Bosnia and Herzegovina

Gheorghe MOZA, Department of Mathematics, Politehnica University Timisoara

Ioan MUȘCUTARIU, Faculty of Physics, West University of Timisoara

Romeo NEGREA, Department of Mathematics, Politehnica University Timisoara

Emilia PETRIȘOR, Department of Mathematics, Politehnica University Timisoara

Mohsen RAZZAGHI, Department of Mathematics and Statistics, Mississippi State Univ., U.S.A.

Ioan ZAHARIE, Department of Physical Fundamentals of Engineering, Politehnica University Timisoara

Please consider, when preparing the manuscript, the Instructions for the Authors at the end of each issue. Orders, exchange for other journals, manuscripts and all correspondences concerning off prints should be sent to the Executive Editors or to the editorial secretaries at the address:

Politehnica University Timisoara
Department of Mathematics
Sq Victoriei 2, 300 006, Timisoara, Romania
Tel.: +40-256-403099 Fax: +40-(0)256-403109

Politehnica University Timisoara
Department of Physical Fundamentals of Engineering,
Bd Vasile Parvan 2, 300223, Timisoara, Romania
Tel.: +40-256-403391 Fax: +40-(0)256-403392

Contents

C. Lăzureanu, J. Cho , On the dynamics of a deformed version of the Shimizu-Morioka system	3
L. F. Vesa , The dynamics of unemployment model with discrete time delay and optimal control	29
T. Cartianu , Some applications of Monte Carlo method in medicine control	38
E. Souca , Application of R software to the data of the comparative study intralesional immunotherapy and cryotherapy in the treatment of warty lesions	51
N. Lupa , Spectral mapping theorem for generalized evolution semigroups	60

ON THE DYNAMICS OF A DEFORMED VERSION OF THE SHIMIZU-MORIOKA SYSTEM

Cristian LĂZUREANU, Jinyoung CHO

Abstract

In this paper, we construct a family of integrable deformations of the Shimizu-Morioka chaotic model. We discuss the stability of a particular deformed system which belongs to this family and we emphasize its chaotic behavior. We also perform some numerical simulations in order to show the transition to chaos and the deformation of the chaotic attractor.¹

1 Introduction

The real life phenomena are often modeled by systems of first order differential equations. Particularly, phenomena with chaotic behavior are widely investigated (see, e.g., [1, 3, 28, 31]) and many chaotic systems were introduced and discussed (see, e.g., [2, 4, 35, 36, 37, 40]). In 1963, Lorenz reported the first chaotic system, so called the Lorenz model [27]. In 1980, Shimizu and Morioka introduced a more tractable model which displays similar dynamics as the Lorenz system [34]. A simplified form of the Shimizu-Morioka system is given by

$$\begin{cases} \dot{x} = y \\ \dot{y} = x - \lambda y - xz \\ \dot{z} = -az + x^2 \end{cases}, \quad (1)$$

where $a, \lambda \in \mathbb{R}$.

System (1) has been investigated from the dynamical point of view, see for instance a partial list of references: chaotic behavior [33, 41], control of chaos [30, 6], bifurcations [38, 26], integrability [11], Jacobi stability [39].

¹MSC(2010): 37D45, 70H05

Keywords and phrases: *Hamilton-Poisson systems, integrable deformation, stability, chaotic systems.*

Recently, integrable deformations of some Hamilton-Poisson systems were discussed (see, e.g., [7, 10, 14, 15, 18, 21, 22, 23, 24]). Moreover, the integrable deformations method for a three-dimensional system of differential equations [16] was applied to some dissipative systems [17, 19, 20]. In this paper, we will apply the above-mentioned method to system (1).

The paper is organized as follows. In Section 2, we construct some integrable deformations of system (1). Then we consider a particular deformation which has the same divergence as the initial system and the same axis of symmetry. In Section 3, we discuss the stability of the new system. More precisely, we get the equilibrium points taking into account the variation of the parameters. Then, we study the stability of the isolated hyperbolic equilibrium points by using the first Lyapunov's stability criterion [25] and Routh-Hurwitz theorem [8]. Also, we establish the stability of the isolated non-hyperbolic equilibrium points by computing the first Lyapunov coefficient (see, e.g., [13]). In Sections 4 and 5, we perform some numerical simulations and point out the chaotic behavior of the considered deformed system.

2 Integrable Deformations of the Shimizu-Morioka system

In this section, we construct some deformation of the Shimizu-Morioka system. Deformations of the system are obtained by using the integrable deformations method for three dimensional systems of differential equations [16].

System (1) writes

$$\dot{\mathbf{x}} = \mathbf{f}(\mathbf{x}),$$

where $\mathbf{x} = (x, y, z) \in \mathbb{R}^3$ and $\mathbf{f}(\mathbf{x}) = (y, x - \lambda y - xz, -az + x^2)$. We choose the vector fields $\mathbf{g}(\mathbf{x})$ and $\mathbf{h}(\mathbf{x})$ such that $\mathbf{f}(\mathbf{x}) = \mathbf{g}(\mathbf{x}) + \mathbf{h}(\mathbf{x})$ and the system $\dot{\mathbf{x}} = \mathbf{g}(\mathbf{x})$ has two functionally independent constants of motion $H = H(\mathbf{x})$ and $C = C(\mathbf{x})$, that is

$$\nabla H \times \nabla C \neq \mathbf{0}, \dot{H} = \dot{C} = 0.$$

We have

$$\mathbf{g}(\mathbf{x}) = (y, x, 0), \quad \mathbf{h}(\mathbf{x}) = (0, -\lambda y - xz, -az + x^2).$$

The system $\dot{\mathbf{x}} = \mathbf{g}(\mathbf{x})$, that is

$$\begin{cases} \dot{x} = y \\ \dot{y} = x \\ \dot{z} = 0 \end{cases},$$

has the constants of the motion

$$H(x, y, z) = z, \quad C(x, y, z) = \frac{1}{2}x^2 - \frac{1}{2}y^2.$$

It is easy to see that $\mathbf{g}(\mathbf{x}) = \nabla H \times \nabla C$. Hence an integrable deformation of system (1) is given by [16]

$$\dot{\mathbf{x}} = \nabla \tilde{H} \times \nabla \tilde{C} + \mathbf{h}(\mathbf{x}), \quad (2)$$

where $\tilde{H} = H + \alpha$, $\tilde{C} = C + \beta$ and α, β are arbitrary differentiable functions on \mathbb{R}^3 . Therefore, we obtain the following result.

Proposition 2.1. *Let α, β be arbitrary differentiable functions on \mathbb{R}^3 . Then a family of integrable deformations of system (1) is given by*

$$\begin{cases} \dot{x} = y - \beta_y + y\alpha_z + \alpha_y\beta_z - \alpha_z\beta_y \\ \dot{y} = x - \lambda y - xz + \beta_x + x\alpha_z - \alpha_x\beta_z + \alpha_z\beta_x \\ \dot{z} = -az + x^2 - y\alpha_x - x\alpha_y + \alpha_x\beta_y - \alpha_y\beta_x \end{cases} \quad (3)$$

where $a, \lambda \in \mathbb{R}$ and $f_x := \frac{\partial f}{\partial x}$.

Particular families of integrable deformations are obtained by choosing the deformation function $\alpha = 0$, that is (3) becomes

$$\begin{cases} \dot{x} = y - \beta_y \\ \dot{y} = x - \lambda y - xz + \beta_x \\ \dot{z} = -az + x^2 - y\alpha_x - x\alpha_y \end{cases} .$$

Also, if $\beta = 0$, then we obtain

$$\begin{cases} \dot{x} = y + y\alpha_z \\ \dot{y} = x - \lambda y - xz + x\alpha_z \\ \dot{z} = -az + x^2 - y\alpha_x - x\alpha_y \end{cases} .$$

We consider the deformation functions $\alpha = \frac{g}{2}z^2$ and $\beta = 0$. System (3) becomes

$$\begin{cases} \dot{x} = y(1 + gz) \\ \dot{y} = x - \lambda y + (g - 1)xz \\ \dot{z} = -az + x^2 \end{cases} , \quad a, \lambda, g \in \mathbb{R}. \quad (4)$$

The first dynamical properties of the above system are given by the next two remarks.

Remark 2.2. *Notice that system (4) has the same divergence as the initial system (1), namely*

$$\nabla \cdot \mathbf{f} = -(a + \lambda).$$

Therefore, if $a + \lambda > 0$, then both systems are dissipative. A dissipative system has "a state space volume that decreases on average along the trajectory so that the orbit approaches an attractor of measure zero in the state space" [36]. In the case of three-dimensional dissipative dynamical systems, these attractors are stable foci, limit cycles, attracting 2-tori, or strange chaotic attractors (see, e.g., [12]).

Remark 2.3. *Shimizu-Morioka system (1) is invariant under the transformation $(x, y, z) \rightarrow (-x, -y, z)$, thus the z -axis is its axis of symmetry. System (4) has the same property. Therefore, a symmetrical orbit or a pair of symmetrical orbits corresponding to symmetrical initial conditions appear in the dynamics of these systems. In addition, the number of the equilibrium points is odd.*

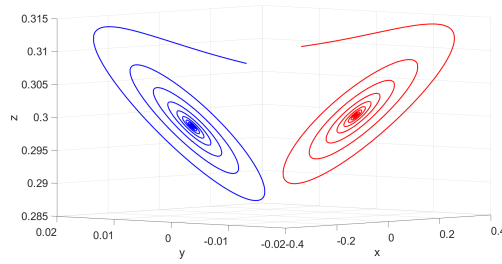


Figure 1: A pair of symmetric stable foci attractors E_1^- and E_1^+ , for $a = 0.34$, $\lambda = 0.77$, $g = -2.34$, with initial conditions $x_0 = x(E_1^-) - 0.01$, $y_0 = y(E_1^-) - 0.01$, $z_0 = z(E_1^-) + 0.01$ (blue) and $x_0 = x(E_1^+) + 0.01$, $y_0 = y(E_1^+) + 0.01$, $z_0 = z(E_1^+) + 0.01$ (red) respectively.

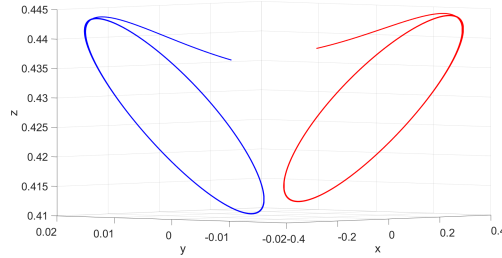


Figure 2: A pair of symmetric limit cycles around E_1^- and E_1^+ , for $a = 0.34$, $\lambda = 0.77$, $g = -1.34$, with initial conditions $x_0 = x(E_1^-) - 0.01$, $y_0 = y(E_1^-) - 0.01$, $z_0 = z(E_1^-) + 0.01$ (blue) and $x_0 = x(E_1^+) + 0.01$, $y_0 = y(E_1^+) + 0.01$, $z_0 = z(E_1^+) + 0.01$ (red) respectively.

System (1) displays some types of the above-mentioned attractors. In Figures 1 and 2 are presented pairs of symmetric stable foci and symmetric stable limit cycles respectively. Also, a symmetric limit cycle is shown in Fig. 3, and a chaotic attractor is plotted in Fig. 9.

In the sequel, we will study the stability of the chaotic behavior of system (4).

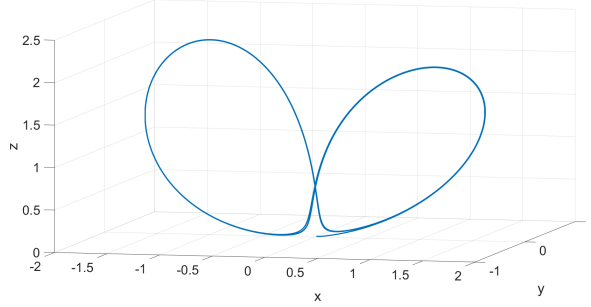


Figure 3: A symmetric limit cycle around E_1^- and E_1^+ , for $a = 0.8$, $\lambda = 1$, $g = 0.14$, with initial conditions $x_0 = 0.01$, $y_0 = 0.01$, $z_0 = 0.01$.

3 Stability

In this section, the equilibrium points of the system (4) are identified, and the stability of these equilibrium points is analyzed.

An equilibrium point of the system $\dot{\mathbf{x}} = \mathbf{f}(\mathbf{x})$ is a stationary point of the system, that is that solution which fulfills the condition

$$(\dot{x}(t), \dot{y}(t), \dot{z}(t)) = (0, 0, 0), \forall t \in \mathbb{R}.$$

Then the equilibrium points of the system (4) are the solutions of the system

$$\begin{cases} y(1 + gz) = 0 \\ x - \lambda y + (g - 1)xz = 0 \\ -az + x^2 = 0 \end{cases} . \quad (5)$$

By solving system (5), we obtain the following equilibrium points of system (4).

Proposition 3.1. *Let $a, \lambda, g \in \mathbb{R}$.*

1. *If $a \neq 0$, $\lambda \neq 0$, $g \notin \{0; 1\}$, $\frac{a}{1-g} < 0$, $\frac{a}{g} > 0$, then the equilibrium point is $O(0, 0, 0)$.*
2. *If $a \neq 0$, $\lambda \neq 0$, $g \notin \{0; 1\}$, $\frac{a}{1-g} > 0$, $\frac{a}{g} > 0$, then the equilibrium points are $O(0, 0, 0)$ and $E_1^\pm \left(\pm \sqrt{\frac{a}{1-g}}, 0, \frac{1}{1-g} \right)$.*
3. *If $a \neq 0$, $\lambda \neq 0$, $g \notin \{0; 1\}$, $\frac{a}{1-g} < 0$, $\frac{a}{g} < 0$, then the equilibrium points are $O(0, 0, 0)$ and $E_2^\pm \left(\pm \sqrt{-\frac{a}{g}}, \pm \frac{1}{\lambda g} \sqrt{-\frac{a}{g}}, -\frac{1}{g} \right)$.*

4. If $a \neq 0$, $\lambda \neq 0$, $g \notin \{0; 1\}$, $\frac{a}{1-g} > 0$, $\frac{a}{g} < 0$, then the equilibrium points are $O(0, 0, 0)$, E_1^\pm , and E_2^\pm .
5. If $a > 0$, $\lambda \neq 0$, $g = 1$, then the equilibrium point is $O(0, 0, 0)$.
6. If $a < 0$, $\lambda \neq 0$, $g = 1$, then the equilibrium points are $O(0, 0, 0)$ and E_2^\pm .
7. If $a > 0$, $\lambda \neq 0$, $g = 0$, then the equilibrium points are $O(0, 0, 0)$ and E_1^\pm .
8. If $a < 0$, $\lambda \neq 0$, $g = 0$, then the equilibrium point is $O(0, 0, 0)$.
9. If $a \neq 0$, $\lambda = 0$, $g = 1$, then the equilibrium point is $O(0, 0, 0)$.
10. If $a \neq 0$, $\lambda = 0$, $g \neq 1$, $\frac{a}{1-g} < 0$, then the equilibrium point is $O(0, 0, 0)$.
11. If $a \neq 0$, $\lambda = 0$, $g \neq 1$, $\frac{a}{1-g} > 0$, then the equilibrium points are $O(0, 0, 0)$ and E_1^\pm .
12. If $a = 0$, $\lambda = 0$, $g = 0$, then the equilibrium points are $E^M(0, 0, M)$, $M \in \mathbb{R}$.
13. If $a = 0$, $\lambda = 0$, $g \neq 0$, then the equilibrium points are $E^M(0, 0, M)$ and $E^N\left(0, N, -\frac{1}{g}\right)$, $M, N \in \mathbb{R}$.
14. If $a = 0$, $\lambda \neq 0$, then the equilibrium points are $E^M(0, 0, M)$, $M \in \mathbb{R}$.

In the following we study the stability of the isolated equilibrium points obtained above. We begin with the stability of $O(0, 0, 0)$.

Proposition 3.2. *For every $a, \lambda, g \in \mathbb{R}$ the equilibrium point $O(0, 0, 0)$ is unstable.*

Proof. The jacobian matrix of system (4) at $O(0, 0, 0)$ is

$$J(0, 0, 0) = \begin{pmatrix} 0 & 1 & 0 \\ 1 & -\lambda & 0 \\ 0 & 0 & -a \end{pmatrix}.$$

The characteristic polynomial is

$$P(\mu) = -(\mu + a)(\mu^2 + \lambda\mu - 1)$$

with eigenvalues

$$\mu_1 = -a, \quad \mu_2 = \frac{-\lambda - \sqrt{\lambda^2 + 4}}{2}, \quad \mu_3 = \frac{-\lambda + \sqrt{\lambda^2 + 4}}{2}.$$

We observe that $\mu_3 > 0$ for all $a, \lambda, g \in \mathbb{R}$. Therefore $O(0, 0, 0)$ is an unstable equilibrium point. \square

In the next result we present the stability of the equilibrium points E_2^\pm .

Proposition 3.3. *If $a \neq 0$, $\lambda \neq 0$, $g \neq 0$, $\frac{a}{g} < 0$, then the equilibrium points $E_2^\pm \left(\pm\sqrt{-\frac{a}{g}}, \pm\frac{1}{\lambda g}\sqrt{-\frac{a}{g}}, -\frac{1}{g} \right)$ are unstable.*

Proof. The jacobian matrix of system (4) at E_2^- and E_2^+ is

$$J(E_2^\pm) = \begin{pmatrix} 0 & 0 & \pm\frac{1}{\lambda}\sqrt{-\frac{a}{g}} \\ \frac{1}{g} & -\lambda & \mp(1-g)\sqrt{-\frac{a}{g}} \\ \pm 2\sqrt{-\frac{a}{g}} & 0 & -a \end{pmatrix}.$$

The characteristic polynomial for both equilibrium points is

$$P(\mu) = -(\mu + \lambda) \left(\mu^2 + a\mu + \frac{2a}{\lambda g} \right)$$

with eigenvalues

$$\mu_1 = -\lambda, \quad \mu_2 = \frac{1}{2} \left(-a - \sqrt{a^2 - \frac{8a}{\lambda g}} \right), \quad \mu_3 = \frac{1}{2} \left(-a + \sqrt{a^2 - \frac{8a}{\lambda g}} \right).$$

1. If $\lambda < 0$, then $\mu_1 > 0$. Thus, the equilibrium points E_2^\pm are unstable.
2. If $\lambda > 0$, then $\mu_1 < 0$ and $\mu_{2,3} \in \mathbb{R}$. We observe that $\mu_3 > 0$ for all $a, \lambda, g \in \mathbb{R}^*$.
Therefore, E_2^\pm are unstable equilibrium points, as required.

□

In the last theorem we discuss the stability of the equilibrium points E_1^\pm .

Theorem 3.4. *Let $a \neq 0$, $\lambda \in \mathbb{R}$, $g \neq 0$, $\frac{a}{1-g} > 0$.*

- (i) *If $\left[a + \lambda > 0, a \left(\lambda^2 + a\lambda - \frac{2}{1-g} \right) > 0 \right]$, then the equilibrium points E_1^\pm are asymptotically stable.*
- (ii) *If $\left[a > 0, \lambda > 0, \lambda^2 + a\lambda - \frac{2}{1-g} = 0, l_1(0) < 0 \right]$, then the equilibrium points E_1^\pm are weak asymptotically stable.*

(iii) If $(a + \lambda \leq 0)$ or $(a\lambda < 0)$ or $\left[a > 0, \lambda > 0, \lambda^2 + a\lambda - \frac{2}{1-g} < 0 \right]$ or $(a > 0, \lambda = 0)$ or $\left[a > 0, \lambda > 0, \lambda^2 + a\lambda - \frac{2}{1-g} = 0, l_1(0) > 0 \right]$, then the equilibrium points E_1^\pm are unstable.

The first Lyapunov coefficient $l_1(0)$ is given by (9).

Proof. The jacobian matrix of system (4) at E_1^- and E_1^+ is

$$J(E_1^\pm) = \begin{pmatrix} 0 & \frac{1}{1-g} & 0 \\ 0 & -\lambda & \mp\sqrt{a(1-g)} \\ \pm 2\sqrt{\frac{a}{1-g}} & 0 & -a \end{pmatrix},$$

with the characteristic equation

$$\mu^3 + (a + \lambda)\mu^2 + a\lambda\mu + \frac{2a}{1-g} = 0. \quad (6)$$

We denote $a_1 = a + \lambda$, $a_2 = a\lambda$, $a_3 = \frac{2a}{1-g}$, whence $a_1 a_2 - a_3 = a \left(\lambda^2 + a\lambda - \frac{2}{1-g} \right)$.

By hypothesis, $a_3 > 0$. Using the Routh-Hurwitz theorem (see, e.g., [8]), we obtain following results:

1. If $a + \lambda > 0$ and $a \left(\lambda^2 + a\lambda - \frac{2}{1-g} \right) > 0$, then the characteristic equation (6) has all roots with negative real part. It follows that E_1^\pm are asymptotically stable equilibrium points.

Hence, (i) is proved.

2. If $a + \lambda < 0$ or $a\lambda < 0$, then the characteristic equation (6) has at least one root with real part strictly positive. Therefore, the equilibrium points E_1^\pm are unstable.
3. If $a + \lambda > 0$, $a\lambda > 0$, and $a \left(\lambda^2 + a\lambda - \frac{2}{1-g} \right) < 0$, then the characteristic equation (6) has a negative real root and a pair of complex conjugate roots with a positive real part. Thus, the equilibrium points E_1^\pm are unstable.
4. If $a + \lambda = 0$, then the characteristic equation (6) has at least one root with real part strictly positive. It follows that the equilibrium points E_1^\pm are unstable.

5. If $a > 0$ and $\lambda = 0$, then the characteristic equation (6) has at least one root with a positive real part. Consequently, the equilibrium points E_1^\pm are unstable.

Hence, the statement (iii) is proved, less the last condition.

Now, let $a \in \mathbb{R}^*$, $\lambda, g \in \mathbb{R}$ be such that

$$a + \lambda > 0, \quad a\lambda > 0, \quad a \left(\lambda^2 + a\lambda - \frac{2}{1-g} \right) = 0.$$

Then $a > 0, \lambda > 0$ and $g = 1 - \frac{2}{\lambda(a + \lambda)}$. Moreover, the characteristic equation (6) has the eigenvalues $\mu_1 = -(a + \lambda)$, $\mu_{2,3} = \pm i\sqrt{a\lambda}$.

In this case, there exist a negative real eigenvalue and a pair of purely imaginary eigenvalues. Therefore, the stability of E_1^- is analyzed by applying the procedures proposed by Kuznetsov [13].

First, we translate the equilibrium point E_1^- into origin. Under the transformation

$$\begin{cases} x = X - \sqrt{\frac{a}{1-g}} \\ y = Y \\ z = Z + \frac{1}{1-g} \end{cases},$$

system (4) becomes

$$\begin{cases} \dot{X} = Y \left(gZ + \frac{1}{1-g} \right) \\ \dot{Y} = -\lambda Y + \sqrt{a(1-g)}Z + (g-1)XZ \\ \dot{Z} = -aZ + X^2 - 2\sqrt{\frac{a}{1-g}}X \end{cases}. \quad (7)$$

The eigenvectors corresponding to eigenvalues $\mu_1 = -(a + \lambda)$, $\mu_2 = -i\sqrt{a\lambda}$, $\mu_3 = i\sqrt{a\lambda}$ are:

$$\begin{aligned} v_1 &= \left(1, -\frac{2}{\lambda}, \sqrt{\frac{2a(a + \lambda)}{\lambda}} \right), \\ v_2 &= \left(1, \frac{-2i}{a + \lambda} \sqrt{\frac{a}{\lambda}}, -(\sqrt{a} + i\sqrt{\lambda}) \sqrt{\frac{2\lambda}{a + \lambda}} \right), \\ v_3 &= \left(1, \frac{2i}{a + \lambda} \sqrt{\frac{a}{\lambda}}, -(\sqrt{a} - i\sqrt{\lambda}) \sqrt{\frac{2\lambda}{a + \lambda}} \right). \end{aligned}$$

We define the vectors

$$T = \operatorname{Re}(v_3) = \left(1, 0, -\sqrt{\frac{2a\lambda}{a+\lambda}} \right),$$

$$W = \operatorname{Im}(v_3) = \left(0, \frac{2}{a+\lambda} \sqrt{\frac{a}{\lambda}}, \lambda \sqrt{\frac{2}{a+\lambda}} \right).$$

Using the vectors $2T$, $-2W$ and v_1 as columns, we construct the matrix

$$B = \begin{pmatrix} 2 & 0 & 1 \\ 0 & -2\beta^2 \sqrt{\frac{a}{\lambda}} & -\frac{2}{\lambda} \\ -2\beta\sqrt{a\lambda} & -2\beta\lambda & \frac{2}{\beta} \sqrt{\frac{a}{\lambda}} \end{pmatrix},$$

where we denote $\beta = \sqrt{\frac{2}{a+\lambda}}$.

Considering the transformation

$$\begin{pmatrix} X \\ Y \\ Z \end{pmatrix} = B \cdot \begin{pmatrix} u \\ v \\ w \end{pmatrix},$$

that is

$$(T) : \begin{cases} X = 2u + w \\ Y = -2\beta^2 \sqrt{\frac{a}{\lambda}} v - \frac{2}{\lambda} w \\ Z = -2\beta\sqrt{a\lambda} u - 2\beta\lambda v + \frac{2}{\beta} \sqrt{\frac{a}{\lambda}} w \end{cases},$$

we get the normal form of system (7), namely

$$\begin{cases} \dot{u} = -\sqrt{a\lambda} v + F_1(u, v, w) \\ \dot{v} = \sqrt{a\lambda} u + F_2(u, v, w) \\ \dot{w} = -(a + \lambda)w + F_3(u, v, w) \end{cases}, \quad (8)$$

where

$$\begin{aligned}
 F_1(u, v, w) &= \gamma A \left[-\beta^3 u - \frac{4\beta(\lambda - \beta^2)}{\lambda^2} \sqrt{\frac{a}{l}} v - \left(\frac{4(\lambda - \beta^2)}{\lambda^3 \beta} + \frac{\beta^3}{2} \right) w \right] \\
 &\quad - \frac{\gamma \beta^2}{2} \sqrt{\frac{a}{\lambda}} (2u + w)^2, \\
 F_2(u, v, w) &= \gamma A \left[\beta \left(\frac{2}{\lambda} + \beta^2 \right) \sqrt{\frac{a}{\lambda}} u + \frac{2\beta^3 a(\lambda - \beta^2)}{\lambda^2} v \right. \\
 &\quad \left. + \left(\frac{\beta}{\lambda} + \frac{\beta^3}{2} + \frac{2\beta(\lambda - \beta^2)}{\lambda^2} \right) \sqrt{\frac{a}{\lambda}} w \right] - \frac{\gamma}{\lambda} (2u + w)^2, \\
 F_3(u, v, w) &= \gamma A \left[2\beta^3 u - \frac{2a\beta^5(\lambda - \beta^2)}{\lambda^2} \sqrt{\frac{a}{l}} v - \left(\frac{2a\beta^3(\lambda - \beta^2)}{\lambda^2} - \beta^3 \right) w \right] + \\
 &\quad \gamma \beta^2 \sqrt{\frac{a}{\lambda}} (2u + w)^2.
 \end{aligned}$$

We have denoted $\gamma = \left(\frac{4}{\lambda\beta} + a\beta^3 \right)^{-1}$, and $A = -2\beta\sqrt{a\lambda}u - 2\beta\lambda v + \frac{2}{\beta}\sqrt{\frac{a}{\lambda}}w$.

By applying procedures and formulas proposed by Hassard [9], the aforementioned coefficients are given by:

$$\begin{aligned}
 g_{11} &= \frac{1}{4} \left[\frac{\partial^2}{\partial u^2} F_1 + \frac{\partial^2}{\partial v^2} F_1 + i \left(\frac{\partial^2}{\partial u^2} F_2 + \frac{\partial^2}{\partial v^2} F_2 \right) \right], \\
 g_{02} &= \frac{1}{4} \left[\frac{\partial^2}{\partial u^2} F_1 - \frac{\partial^2}{\partial v^2} F_1 - 2 \frac{\partial^2}{\partial u \partial v} F_2 + i \left(\frac{\partial^2}{\partial u^2} F_2 - \frac{\partial^2}{\partial v^2} F_2 + 2 \frac{\partial^2}{\partial u \partial v} F_1 \right) \right], \\
 g_{20} &= \frac{1}{4} \left[\frac{\partial^2}{\partial u^2} F_1 - \frac{\partial^2}{\partial v^2} F_1 + 2 \frac{\partial^2}{\partial u \partial v} F_2 + i \left(\frac{\partial^2}{\partial u^2} F_2 - \frac{\partial^2}{\partial v^2} F_2 - 2 \frac{\partial^2}{\partial u \partial v} F_1 \right) \right], \\
 h_{11} &= \frac{1}{4} \left[\frac{\partial^2}{\partial u^3} F_3 + \frac{\partial^2}{\partial v^3} F_3 \right], \quad h_{20} = \frac{1}{4} \left[\frac{\partial^2}{\partial u^3} F_3 - \frac{\partial^2}{\partial v^3} F_3 - 2i \frac{\partial^2}{\partial u \partial v} F_3 \right], \\
 w_{11} &= -\frac{h_{11}}{\mu_1}, \quad w_{20} = \frac{h_{20}}{2i\alpha_0 - \mu_1}, \\
 G_{10} &= \frac{1}{2} \left[\frac{\partial^2}{\partial u \partial w} F_1 + \frac{\partial^2}{\partial v \partial w} F_2 + i \left(\frac{\partial^2}{\partial u \partial w} F_2 - \frac{\partial^2}{\partial v \partial w} F_1 \right) \right], \\
 G_{01} &= \frac{1}{2} \left[\frac{\partial^2}{\partial u \partial w} F_1 - \frac{\partial^2}{\partial v \partial w} F_2 + i \left(\frac{\partial^2}{\partial u \partial w} F_2 + \frac{\partial^2}{\partial v \partial w} F_1 \right) \right], \\
 G_{21} &= \frac{1}{8} \left[\frac{\partial^3}{\partial u^3} F_1 + \frac{\partial^3}{\partial u \partial v^2} F_1 + \frac{\partial^3}{\partial u^2 \partial v} F_2 + \frac{\partial^3}{\partial v^3} F_2 \right. \\
 &\quad \left. + i \left(\frac{\partial^3}{\partial u^3} F_2 + \frac{\partial^3}{\partial u \partial v^2} F_2 - \frac{\partial^3}{\partial u^2 \partial v} F_1 - \frac{\partial^3}{\partial v^3} F_1 \right) \right], \\
 g_{21} &= G_{21} + 2G_{10}w_{11} + G_{01}w_{20}.
 \end{aligned}$$

where $\alpha_0 = \text{Im}(\mu_3)$.

The first Lyapunov coefficient for E_1^- is given by

$$l_1(0) = \frac{1}{2a\lambda} \text{Re} \left(ig_{20}g_{11} + g_{21}\sqrt{a\lambda} \right), \quad (9)$$

where

$$\begin{aligned} g_{11} &= \frac{\gamma}{\lambda} \left[\frac{\beta^2\sqrt{a}(\beta^2\lambda^2 - 4\beta^2 + 3\lambda)}{\sqrt{\lambda}} + i(2a\beta^6 - 3a\beta^4\lambda - 2a\beta^2 - 2) \right], \\ g_{02} &= \frac{\gamma}{\lambda} \left[\frac{-\beta^2\sqrt{a}(2a\beta^4 - 2a\beta^2\lambda - 2\beta^2\lambda^2 - 4\beta^2 + 3\lambda)}{\sqrt{\lambda}} \right. \\ &\quad \left. - i \left(\frac{2a\beta^6\lambda - a\beta^4\lambda^2 - \beta^4\lambda^3 + 4a\beta^4 - 2a\beta^2\lambda + 2\lambda}{\lambda} \right) \right], \\ g_{20} &= \frac{\gamma}{\lambda} \left[\frac{\beta^2\sqrt{a}(2a\beta^4 - 2a\beta^2\lambda + 4\beta^2 - 7\lambda)}{\sqrt{\lambda}} \right. \\ &\quad \left. - i \left(\frac{2a\beta^6\lambda - a\beta^4\lambda^2 + \beta^4\lambda^3 - 4a\beta^4 + 6a\beta^2\lambda + 2\lambda}{\lambda} \right) \right], \\ h_{11} &= -\frac{2\gamma\beta^2\sqrt{a}(a\beta^6 - a\beta^4\lambda + \beta^2\lambda - 1)}{\sqrt{\lambda}}, \\ h_{20} &= \frac{\gamma}{\sqrt{\lambda}} \left[2\beta^2\sqrt{a}(a\beta^6 - a\beta^4\lambda - \beta^2\lambda + 1) + i \left(\frac{2\beta^4(a^2\beta^4 - a^2\beta^2\lambda + \lambda^2)}{\sqrt{\lambda}} \right) \right], \\ w_{11} &= \frac{\beta^2}{2} h_{11}, \\ w_{20} &= \frac{\beta^2(1 - i\beta^2\sqrt{a\lambda})}{2(1 + a\lambda\beta^4)} h_{20}, \\ G_{10} &= -\frac{\gamma\sqrt{a}(2a\beta^4 - 2\beta^4\lambda - 2a\beta^2\lambda + 5\beta^2\lambda^2 + 4\beta^2 - 4\lambda)}{\lambda^2\sqrt{\lambda}} - \\ &\quad i \left[\frac{\gamma(a\beta^4\lambda^3 + \beta^4\lambda^4 - 4a\beta^4\lambda + 4a\beta^2\lambda^2 + 8a\beta^2 - 8\beta^2\lambda - 12a\lambda + 12\lambda^2)}{2\lambda^3} \right], \\ G_{01} &= \frac{\gamma\sqrt{a}(\beta^4\lambda^3 + 2a\beta^4 - 2\beta^4\lambda - 2a\beta^2\lambda + \beta^2\lambda^2 - 4\beta^2 + 4\lambda)}{\lambda^2\sqrt{\lambda}} - \\ &\quad i \left[\frac{\gamma(a\beta^4\lambda^3 - \beta^4\lambda^4 - 4a\beta^4\lambda + 4a\beta^2\lambda^2 - 8a\beta^2 + 8\beta^2\lambda + 4a\lambda - 4\lambda^2)}{2\lambda^3} \right], \\ G_{21} &= 0, \\ g_{21} &= 2G_{10}w_{11} + G_{01}w_{20}. \end{aligned}$$

By using the same arguments and procedures as before, the stability of E_1^+ is analyzed. By the substitution

$$\begin{cases} x = -X + \sqrt{\frac{a}{1-g}} \\ y = -Y \\ z = Z + \frac{1}{1-g} \end{cases},$$

system (4) becomes (7). Therefore, we get the same first Lyapunov coefficient.

Taking into account the sign of $l_1(0)$, we obtain (ii) and the last assertion of (iii), which finishes the proof. \square

4 Chaotic behavior

In this section, computer simulations point out the chaotic behavior of the system (4). In addition, evolutions of the largest Lyapunov exponent and the Kaplan - York dimension of the system (4) are analyzed.

Following [42], recall that the signs of the Lyapunov exponents give a qualitative picture of the dynamics of a system. The sum of the three Lyapunov exponents of a three-dimensional continuous dissipative dynamical system is negative, and consequently at least one Lyapunov exponent is negative. A positive Lyapunov exponent of a bounded attractor indicates the exponential expansion of the trajectory, hence "the system experiences repeated stretching and folding", which leads to a strange attractor.

The Lyapunov exponents μ_1, μ_2, μ_3 constitute the Lyapunov exponent spectrum, and their signs form the symbolic Lyapunov spectrum. For example, if $\mu_1 > 0, \mu_2 = 0, \mu_3 < 0$, then the corresponding element of the symbolic Lyapunov spectrum is the triple $(+, 0, -)$. "In a three-dimensional continuous dissipative dynamical system the only possible spectra, and the attractors they describe, are as follows: $(+, 0, -)$, a strange attractor; $(0, 0, -)$, a two-torus; $(0, -, -)$, a limit cycle; and $(-, -, -)$, a fixed point." [42]

In the sequel, we explore the variation of the largest Lyapunov exponent.

Consider the parameters a and λ fixed, namely $a = 0.45, \lambda = 0.75$. Using E&F Chaos program [5], in Figure 4, the variation of the largest Lyapunov exponent with respect to parameter g is presented. We can also see that the maximum value for the largest Lyapunov exponent is obtained for $g = 0.92$.

Now, we set the parameters $\lambda = 0.75$ and $g = 0.92$. In Figure 5, the variation of the largest Lyapunov exponent with respect to parameter λ is shown. In this case, the maximum value for the largest Lyapunov exponent is obtained for $a = 0.34$.

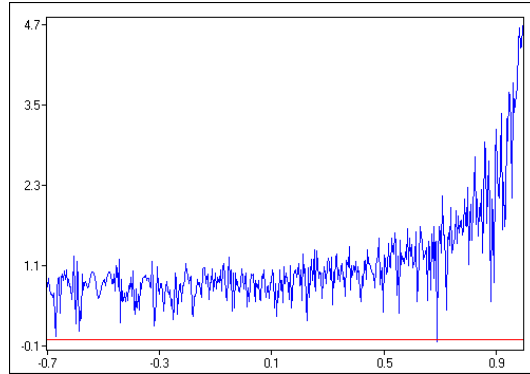


Figure 4: The variation of the largest Lyapunov exponent with respect to the parameter g ($a = 0.45$, $\lambda = 0.75$, $x_0 = 0.01$, $y_0 = 0.01$, $z_0 = 0.01$).

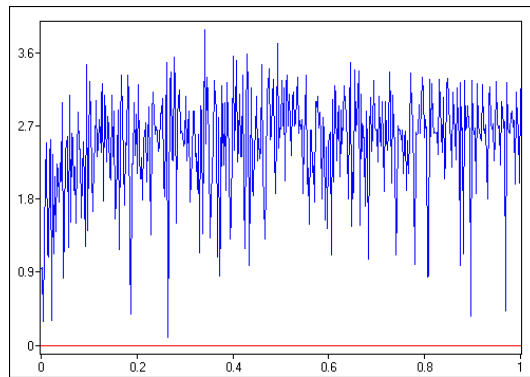


Figure 5: The variation of the largest Lyapunov exponent with respect to the parameter a ($\lambda = 0.75$, $g = 0.92$, $x_0 = 0.01$, $y_0 = 0.01$, $z_0 = 0.01$).

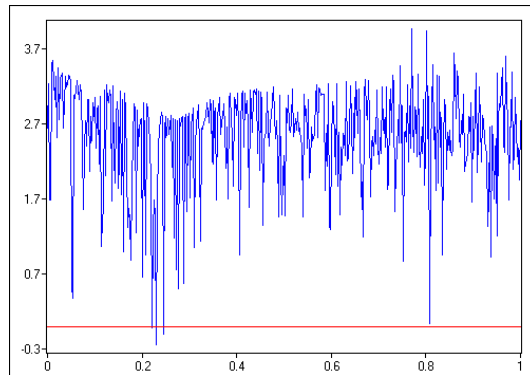


Figure 6: The variation of the largest Lyapunov exponent with respect to the parameter λ ($a = 0.45$, $g = 0.92$, $x_0 = 0.01$, $y_0 = 0.01$, $z_0 = 0.01$).

Finally, in Figure 6, for $a = 0.45$ and $g = 0.92$, the variation of the largest Lyapunov exponent with respect to parameter λ is presented. In the last simulation, the maximum value for the largest Lyapunov exponent is obtained for $\lambda = 0.77$.

In the following we compare some chaotic indicators of the Shimizu-Morioka system and its deformation (4).

Recall that Shimizu-Morioka system (1) is chaotic for $a = 0.45, \lambda = 0.75$ (see, e.g., [33]). The corresponding attractor is drawn in Fig. 15(a).

Using "LCE package for Mathematica" [32], setting $a = 0.45, \lambda = 0.75$ and $g = 0$ in system (4) with the initial conditions $x_0 = 0.01, y_0 = 0.01, z_0 = 0.01$, the largest Lyapunov exponent is $\mu_1 = 0.0637008$. In addition, the other Lyapunov exponents are $\mu_2 \simeq 0, \mu_3 = -1.264$.

Setting $a = 0.34, \lambda = 0.77$ and $g = 0.92$ in system (4) with the initial conditions $x_0 = 0.01, y_0 = 0.01, z_0 = 0.01$, the largest Lyapunov exponent is $\mu_1 = 0.407006$. The other Lyapunov exponents are $\mu_2 \simeq 0, \mu_3 = -1.51811$.

The Lyapunov dimension or Kaplan-Yorke dimension of a chaotic attractor of a three-dimensional system is

$$D_L = 2 + \frac{\mu_1 + \mu_2}{|\mu_3|}.$$

Therefore $D_L = 2.05064$ for $a = 0.45, \lambda = 0.75, g = 0$ and $D_L = 2.26883$ for $a = 0.34, \lambda = 0.77, g = 0.92$

In Figure 7, the convergence plot of the Lyapunov spectrum for system (4) is presented.

Using Matlab R2023a, the time series (Fig. 8), the trajectory of the system (4) for $a = 0.34, \lambda = 0.77, g = 0.92$ (Fig. 9) and its projections on the coordinates planes (Fig. 10) are shown.

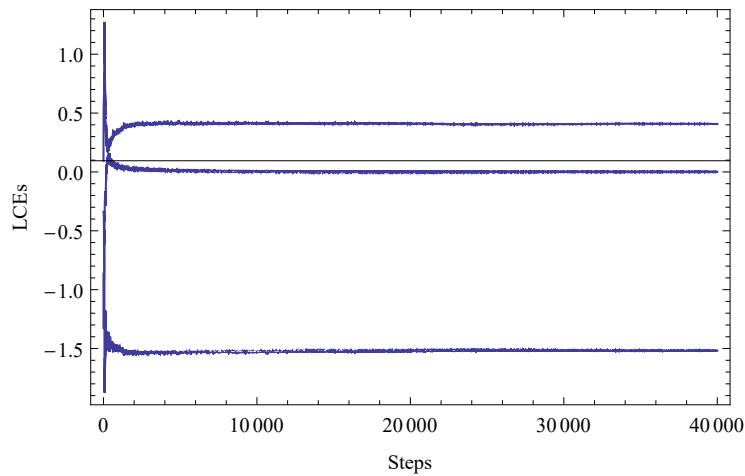


Figure 7: Convergence plot of the Lyapunov spectrum for system (4) ($a = 0.34, \lambda = 0.77, g = 0.92, x_0 = 0.01, y_0 = 0.01, z_0 = 0.01$).

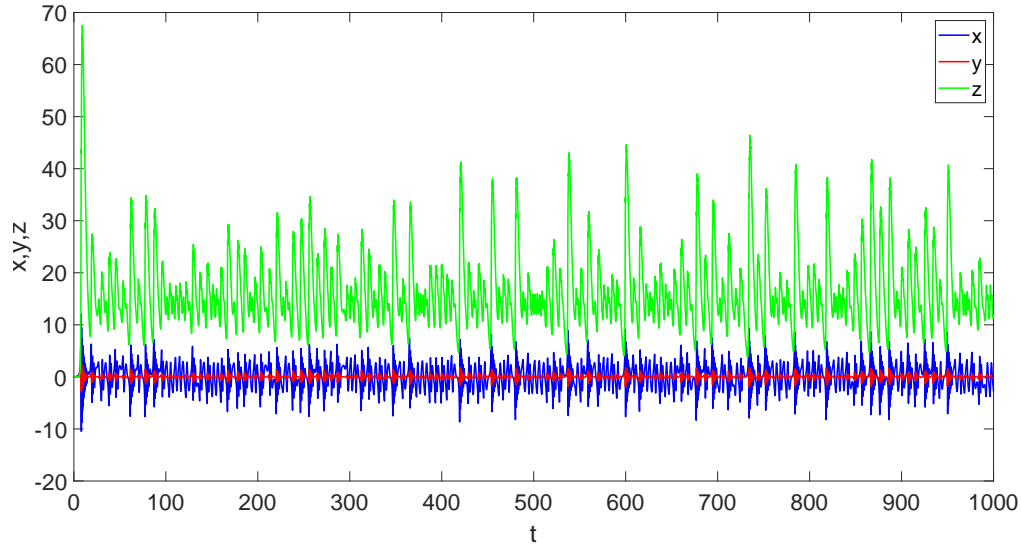


Figure 8: The time series of a chaotic attractor of system (4) for $a = 0.34$, $\lambda = 0.77$, $g = 0.92$, with the initial conditions $x_0 = 0.01$, $y_0 = 0.01$, $z_0 = 0.01$.

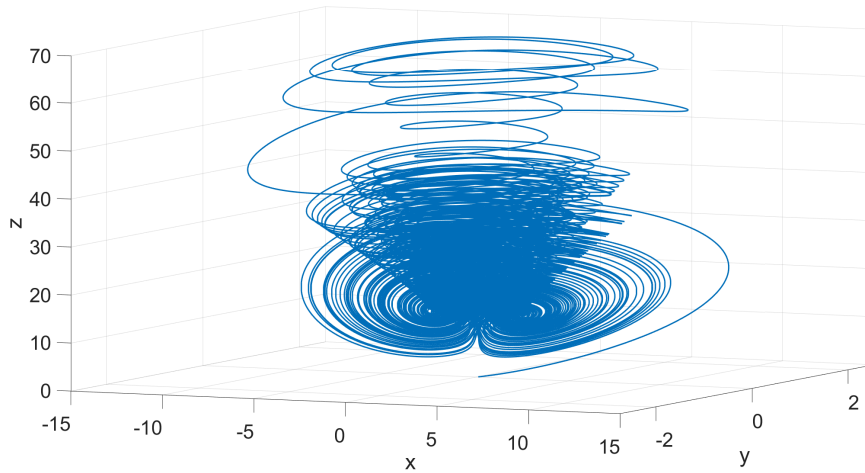
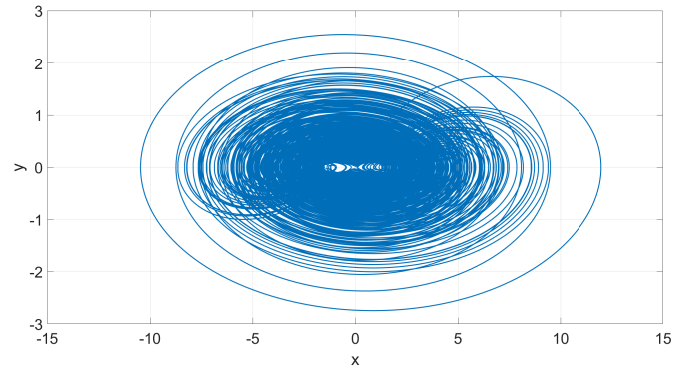


Figure 9: A chaotic attractor of system (4) for $a = 0.34$, $\lambda = 0.77$, $g = 0.92$, with the initial conditions $x_0 = 0.01$, $y_0 = 0.01$, $z_0 = 0.01$.

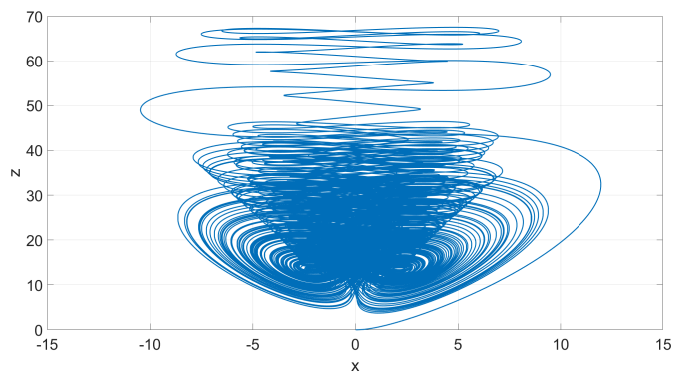
5 Numerical simulations

In this section, using Matlab R2023a, we give some numerical simulations of the trajectory of system (4) (see Figures 11-16).

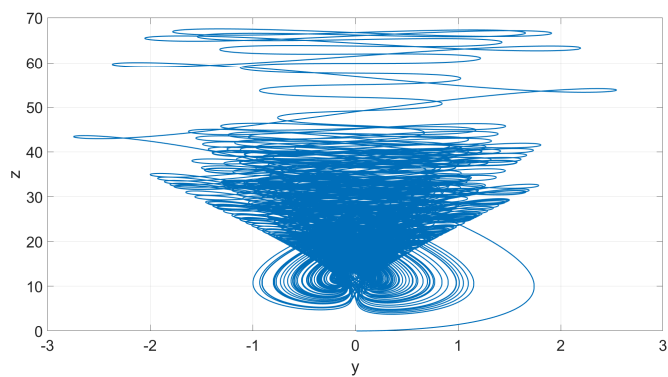
We start with a route of chaos of the considered system in the case $a = 0.8$, $\lambda = 0.934$, and g varying between -0.8 and 0.9 . An asymptotically stable attractor



(a) projection on the x-y plane



(b) projection on the x-z plane



(c) projection on the y-z plane

Figure 10: The projections of the chaotic attractor of system (4) on the coordinates planes ($a = 0.34$, $\lambda = 0.77$, $g = 0.92$, $x_0 = 0.01$, $y_0 = 0.01$, $z_0 = 0.01$).

(Fig. 11(a)) turns into a limit cycle (Fig. 11(b)), which is stable (Fig. 11(c)). This limit cycle deforms into a homoclinic orbit (Fig. 11(d)). Because system (4) has a rotational symmetry around Oz -axis, there is in fact a pair of homoclinic orbits, which give rise to a symmetric limit cycle (Fig. 11(e)), which is also stable (Fig. 11(f)). Note that these homoclinic orbits (in the case $g = 0$) were reported in [33]. The moment of the appearance of a strange attractor is shown in Fig. 12(b). The evolution of this attractor is presented in Figures 12(c)-12(h).

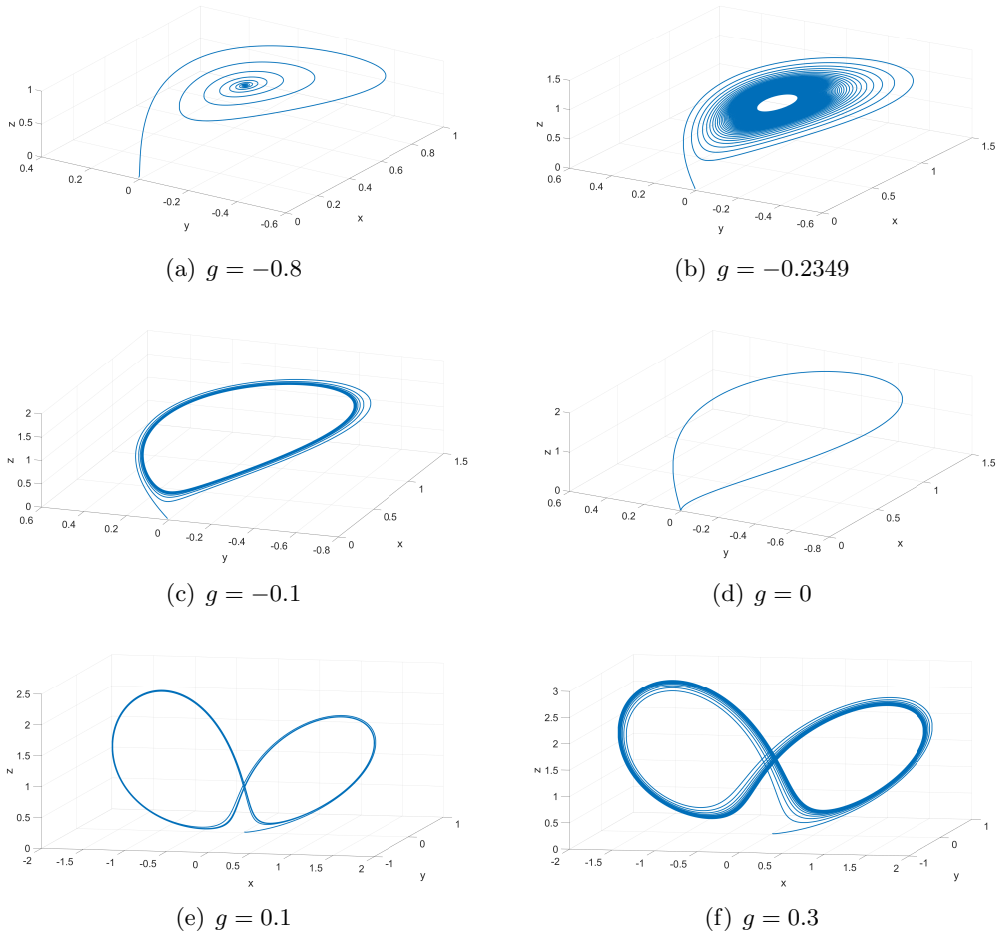
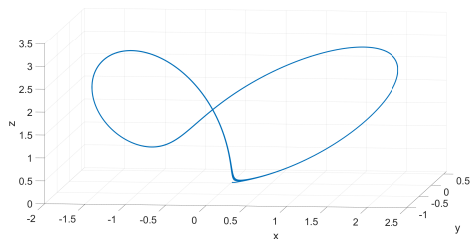
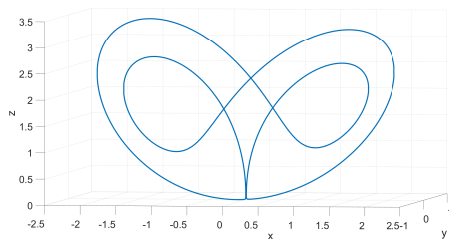


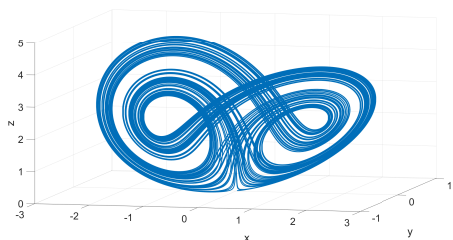
Figure 11: A deformation of system (4) ($a = 0.8$, $\lambda = 0.934$, $x_0 = 0.01$, $y_0 = 0.01$, $z_0 = 0.01$).



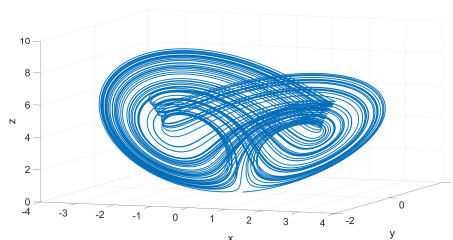
(a) $g = 0.38$



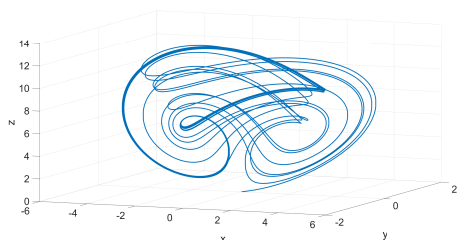
(b) $g = 0.383$



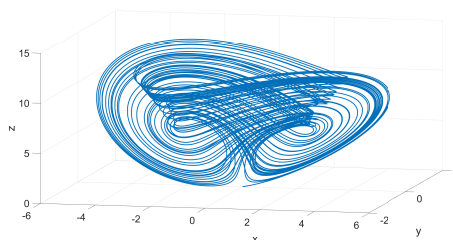
(c) $g = 0.5$



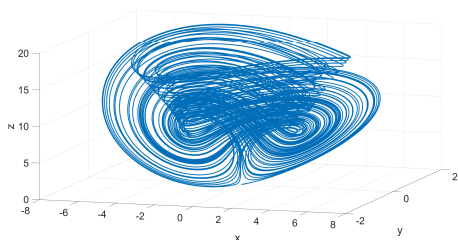
(d) $g = 0.7$



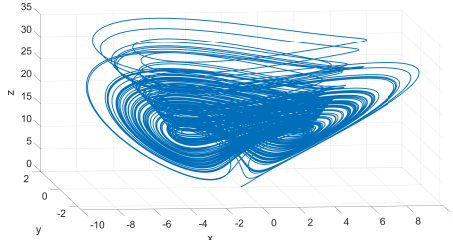
(e) $g = 0.798$



(f) $g = 0.799$



(g) $g = 0.85$



(h) $g = 0.9$

Figure 12: The continuation of Fig. 11: A deformation of system (4) ($a = 0.8$, $\lambda = 0.934$, $x_0 = 0.01$, $y_0 = 0.01$, $z_0 = 0.01$).

Another transition between an asymptotically stable attractor and a strange attractor is presented in Figures 13 and 14. We set $a = 0.14$, $\lambda = 2$, and vary g between 0 and 0.9. For $g = 0$ system (4) has an asymptotically stable attractor (E_1^- , Fig. 13(a)) and before $g = 4$ it turns into another asymptotically stable attractor (E_1^+ , Fig. 13(b)). Finally, another strange attractor is point out (Fig. 14(h)).

In Fig. 15, we present the transition of the Shimizu-Morioka chaotic attractor (Fig. 15(a)), which looks as the Lorenz attractor [27], to the new chaotic attractor (4) (Fig. 15(e)), which looks as the Chen attractor [4].

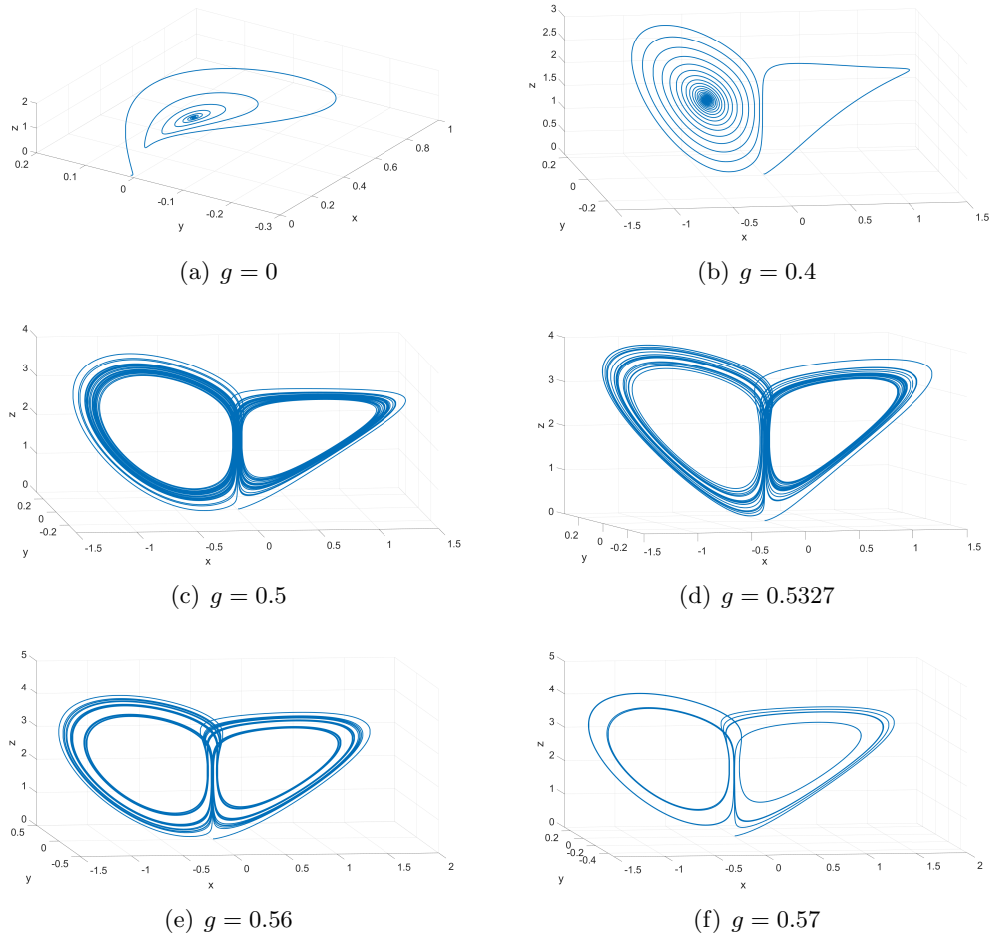
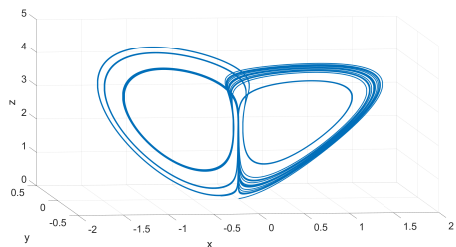
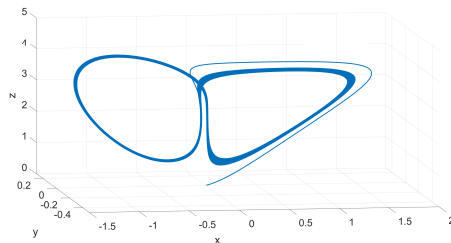


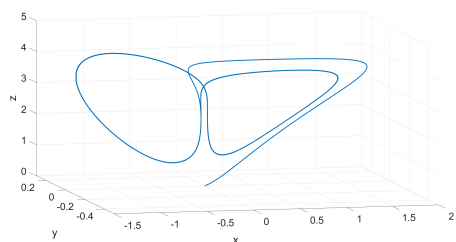
Figure 13: A deformation of system (4) ($a = 0.14$, $\lambda = 2$, $x_0 = 0.01$, $y_0 = 0.01$, $z_0 = 0.01$).



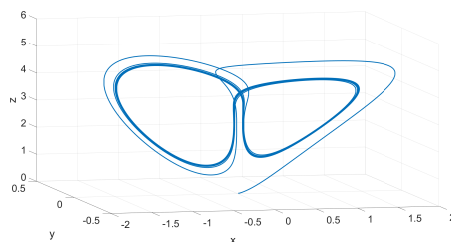
(a) $g = 0.58$



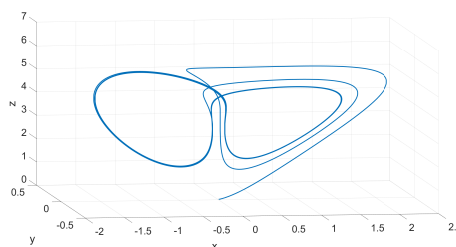
(b) $g = 0.59$



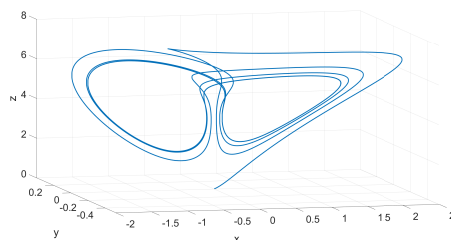
(c) $g = 0.6$



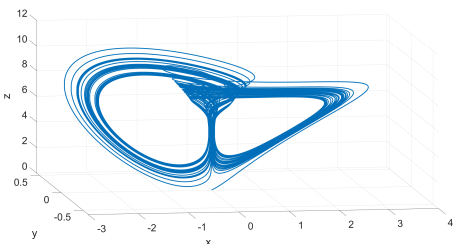
(d) $g = 0.65$



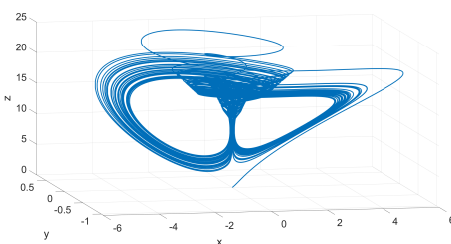
(e) $g = 0.7$



(f) $g = 0.75$



(g) $g = 0.8$



(h) $g = 0.9$

Figure 14: The continuation of Fig. 13: A deformation of system (4) ($a = 0.14$, $\lambda = 2$, $x_0 = 0.01$, $y_0 = 0.01$, $z_0 = 0.01$).

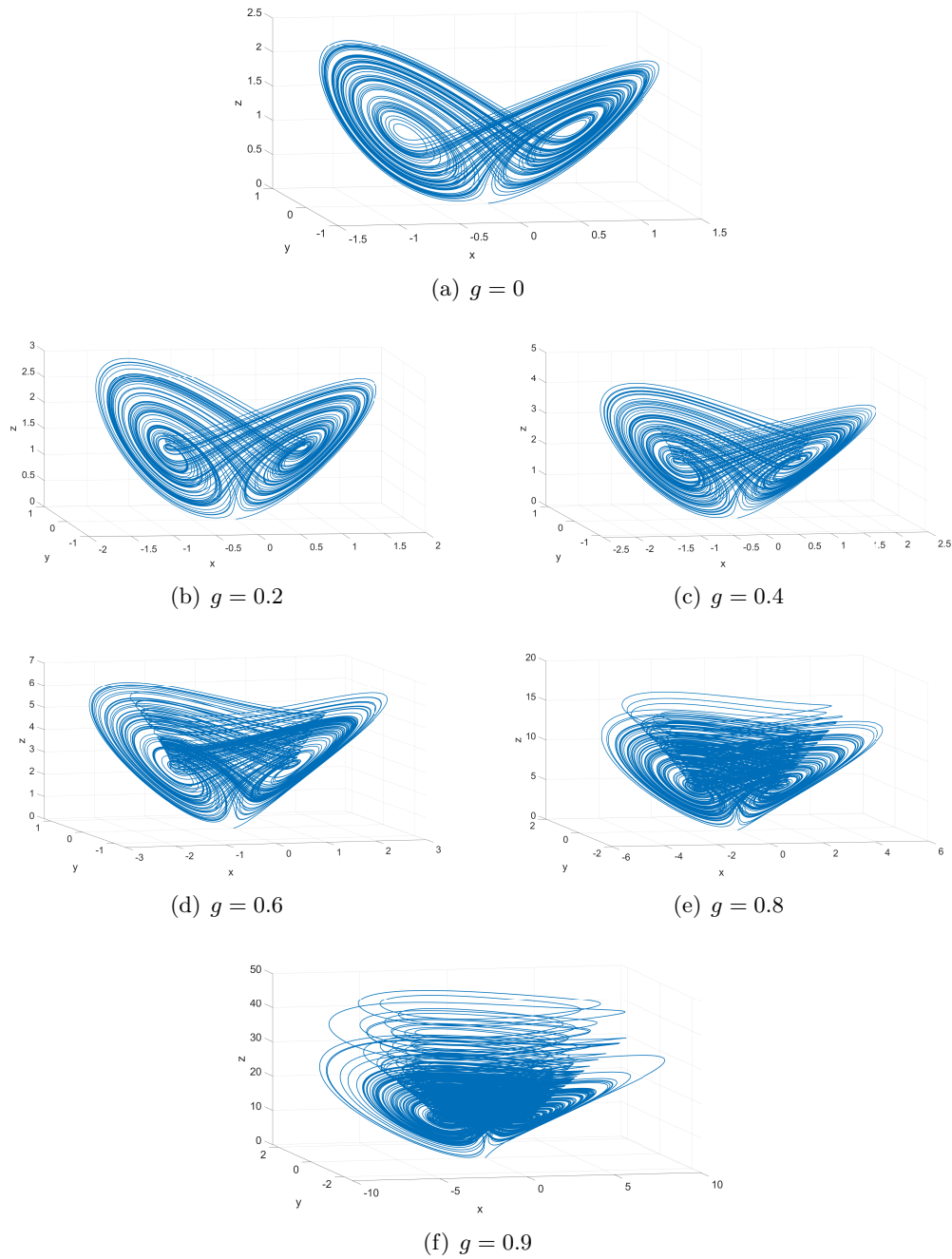


Figure 15: Deformations of the Shimizu-Morioka chaotic attractor (4) ($a = 0.45$, $\lambda = 0.75$, $x_0 = 0.01$, $y_0 = 0.01$, $z_0 = 0.01$).

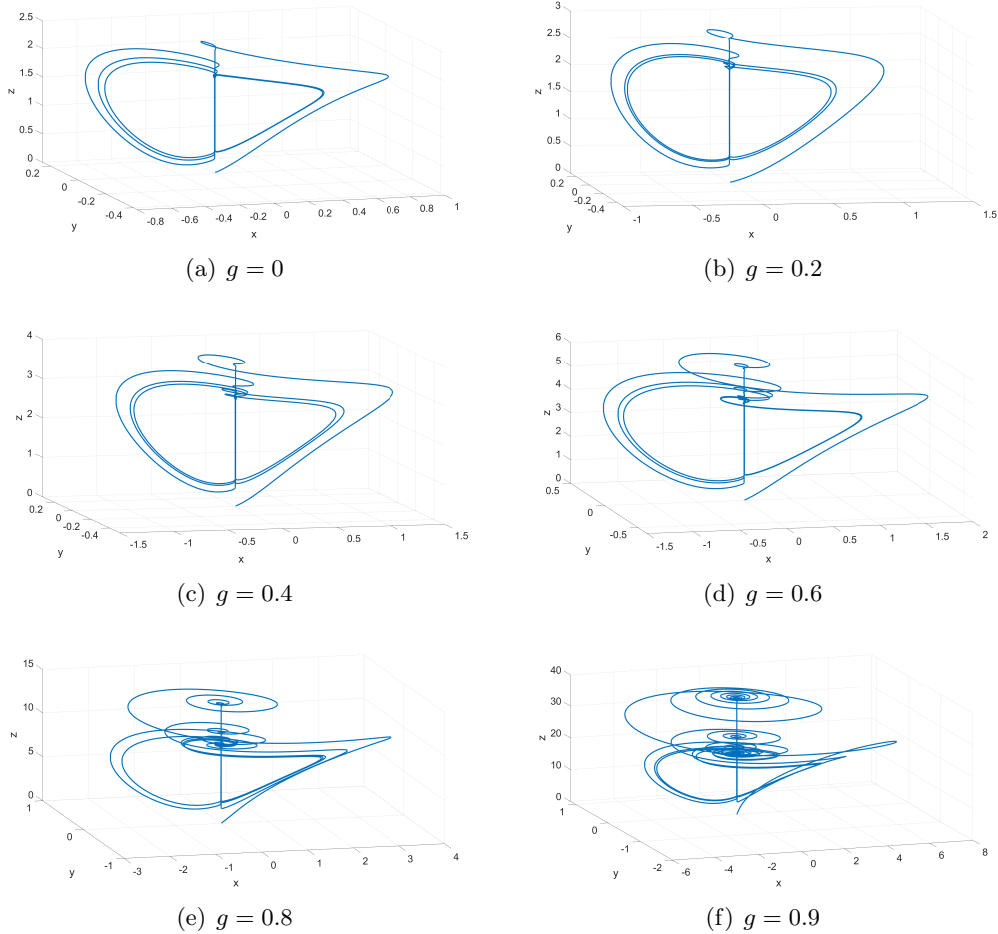


Figure 16: A chaotic deformation of system (4) for (a) $g = 0$; (b) $g = 0.2$; (c) $g = 0.4$; (d) $g = 0.6$; (e) $g = 0.8$; (f) $g = 0.9$. ($a = 0.01$, $\lambda = 1.4$, $x_0 = 0.01$, $y_0 = 0.01$, $z_0 = 0.01$).

References

- [1] A. Babloyantz, C. Nicolis, J.M. Salazar, Evidence of chaotic dynamics of brain activity during the sleep cycle, *Physics Letters A*, **111**, (1985), 152–156.
- [2] T. Bînzar, C. Lăzureanu, On a new chaotic system, *Mathematical Methods in the Applied Sciences*, **38**(8), (2015), 1631–1641.
- [3] G. Chen, Controlling Chaos and Bifurcations in Engineering Systems, *CRC Press, Boca Raton, FL*, 1999.
- [4] G. Chen, T. Ueta, Yet another chaotic attractor, *International Journal of Bifurcation and Chaos*, **9**, (1999), 1465–1466.

- [5] C. Diks, C.H. Hommes, V. Panchenko, R. van der Weide, E&F chaos: A user friendly software package for nonlinear economic dynamics, *Computational Economics*, **32**, (2008), 221—244.
- [6] M.M. El-Dessoky, M.T. Yassen, E.S. Aly, Bifurcation analysis and chaos control in Shimizu-Morioka chaotic system with delayed feedback, *Applied Mathematics and Computation*, **243**, (2014), 283—297.
- [7] A. Galajinsky, Remark on integrable deformations of the Euler top, *Journal of Mathematical Analysis and Applications*, **416**(2), (2014), 995–997.
- [8] F.R. Gantmacher, *Matrix Theory*, Chelsea Pub. Co., New York, NY, USA, 2000, Volume 2.
- [9] B. Hassard, Y.H. Wan, Bifurcation formulae derived from center manifold theory, *Journal of Mathematical Analysis and Applications*, **63**, (1978), 297–312.
- [10] K. Huang, S. Shi, Z. Xu: Integrable deformations, bi-Hamiltonian structures and nonintegrability of a generalized Rikitake system, *International Journal of Geometric Methods in Modern Physics*, **16**(4), (2019), 1950059.
- [11] K. Huang, S. Shi, W. Li., Integrability analysis of the Shimizu–Morioka system, *Communications in Nonlinear Science and Numerical Simulation*, **84**, (2020), 105101.
- [12] W. Kinsner, Characterizing chaos through lyapunov metrics, *IEEE Transactions on Systems, Man and Cybernetics, Part C (Applications and Reviews)*, **36**(2), (2006), 141–151.
- [13] Y.A. Kuznetsov, *Elements of Applied Bifurcation Theory*, Springer-Verlag: New York, NY, USA, 1998.
- [14] C. Lăzureanu, On the Hamilton-Poisson realizations of the integrable deformations of the Maxwell-Bloch equations, *Comptes Rendus Mathématique*, **355**, (2017), 596–600.
- [15] C. Lăzureanu, Hamilton-Poisson Realizations of the Integrable Deformations of the Rikitake System, *Advances in Mathematical Physics*, **2017**, (2017), 4596951.
- [16] C. Lăzureanu, Integrable Deformations of Three-Dimensional Chaotic Systems, *International Journal of Bifurcation and Chaos*, **28**(5), (2018), 1850066.
- [17] C. Lăzureanu, Chaotic behavior of an integrable deformation of a nonlinear monetary system, *AIP Conference Proceedings* 2116, (2019), 370004.
- [18] C. Lăzureanu, Integrable Deformations and Dynamical Properties of Systems with Constant Population, *Mathematics*, **9**, (2021), 1378.

- [19] C. Lăzureanu, Dynamical Properties, Deformations, and Chaos in a Class of Inversion Invariant Jerk Equations, *Symmetry*, **14**, (2022), 1318.
- [20] C. Lăzureanu, C. Căplescu, On a deformed version of the T system, *Proceedings of The XV-th International Conference on Mathematics and its Applications*, Timișoara, 2019, 90–97.
- [21] C. Lăzureanu, C. Hedrea, C. Petrișor, Stability and some special orbits for an integrable deformation of the Rikitake system, *2018 International Conference on Applied Mathematics & Computer Science (ICAMCS)*, Paris, France, 2018, 1–18.
- [22] C. Lăzureanu, C. Hedrea, C. Petrișor, On the integrable deformations of a system related to the motion of two vortices in an ideal incompressible fluid, *International Conference on Computational Methods and Applications in Engineering (ICCMAE 2018)*, Timișoara, Romania, 2018, ITM Web of Conferences **29**, (2019), 01015.
- [23] C. Lăzureanu, C. Petrișor, Stability and Energy-Casimir Mapping for Integrable Deformations of the Kermack-McKendrick System, *Advances in Mathematical Physics*, **2018**, (2018), 5398768.
- [24] C. Lăzureanu, C. Petrișor, C. Hedrea, On a Deformed Version of the Two-Disk Dynamo System, *Applications of Mathematics*, **66**, (2021), 345–372.
- [25] A.M. Lyapunov, *Problème Générale de la Stabilité du Mouvement*, Princeton University Press, Princeton, NJ, USA, 1949, Volume 17.
- [26] J. Llibre, C. Pessoa, The Hopf bifurcation in the Shimizu-Morioka system, *Nonlinear Dynamics*, **79**, (2015), 2197–2205.
- [27] E.N. Lorenz, Deterministic nonperiodic flow, *Journal of the Atmospheric Sciences*, **20**(2), (1963), 130–141.
- [28] L.M. Pecora, T.L. Carroll, Driving systems with chaotic signals, *Physical Review A*, **44**(4), (1991), 2374–83.
- [29] L. Perko, *Differential Equations and Dynamical Systems*, 3rd ed., Texts in Applied Mathematics 7, Springer-Verlag: New York, NY, USA, 2001.
- [30] K. Pyragas, Continuous control of chaos by self-controlling feedback, *Physics Letters A*, **170**(6), (1992), 421–8.
- [31] M.I. Rabinovich, H.D.I. Abarbanel, The role of chaos in neural systems, *Neuroscience*, **87**, (1998), 5–14.
- [32] M. Sandri, LCE package for Mathematica 7, (2010), <http://www.msandri.it>.

- [33] A.L. Shil'nikov, On bifurcations of the Lorenz attractor in the Shimizu-Morioka model, *Physica D: Nonlinear Phenomena*, **62**(1-4), (1993), 338–346.
- [34] T. Shimizu, N. Morioka, On the bifurcation of a symmetric limit cycle to an asymmetric one in a simple model, *Physics Letters A*, **76**(3-4), (1980), 201–204.
- [35] J.C. Sprott, X. Wang, G. Chen, Coexistence of point, periodic and strange attractors, *International Journal of Bifurcation and Chaos*, **23**(5), (2013), 1350093.
- [36] J.C. Sprott, A dynamical system with a strange attractor and invariant tori, *Physics Letters A*, **378**, (2014), 1361–1363.
- [37] G. Tigan, Analysis of a dynamical system derived from the Lorenz system, *Scientific Bulletin of the Politehnica University of Timisoara*, **50**(64)(1), (2005), 61–72.
- [38] G. Tigan, D. Turaev, Analytical search for homoclinic bifurcations in the Shimizu-Morioka model. *Physica D: Nonlinear Phenomena*, **240**(12), (2011), 985–9.
- [39] X. Zhang, When Shimizu-Morioka model meets Jacobi stability analysis: Detecting chaos, *International Journal of Geometric Methods in Modern Physics*, **20**(2), (2023), 2350033.
- [40] Z. Wei, J.C. Sprott, H. Chen, Elementary quadratic chaotic flows with a single non-hyperbolic equilibrium, *Physics Letters A* **2015**, 379, 2184–2187.
- [41] Z. Wei, X. Zhang, Chaos in the Shimizu-Morioka Model With Fractional Order, *Frontiers in Physics*, **9**, (2021), 636173.
- [42] A. Wolf, J.B. Swift, H.L. Swinney, J.A. Vastano, Determining Lyapunov exponents from a time series, *Physica D: Nonlinear Phenomena*, **16**(3), (1995), 285–317.

Cristian Lăzureanu – Department of Mathematics,
Politehnica University of Timișoara,
P-ta Victoriei 2, 300 006, Timișoara, ROMANIA
E-mail: cristian.lazureanu@upt.ro

Jinyoung Cho – MSc student, Department of Mathematics,
Politehnica University of Timișoara,
P-ta Victoriei 2, 300 006, Timișoara, ROMANIA
E-mail: jinyoung.cho@student.upt.ro

THE DYNAMICS OF AN UNEMPLOYMENT MODEL WITH DISCRETE TIME DELAY AND OPTIMAL CONTROL

Loredana Flavia VESA

Abstract

The purpose of this paper is to analyzed a mathematical model of three ordinary differential equations which describe the unemployment incorporating a discrete time delay and optimal control. The model's investigation focuses on assessing the stability analysis of the equilibrium point as well as the optimal control. Theoretical statements are supported by conducting numerical simulations. ²

1 Introduction

Comprehending the dynamic nature of social issues is crucial in developing effective solutions, particularly in the case of unemployment, which is a pervasive concern impacting individuals worldwide. As an essential indicator of a nation's economic status, gaining a comprehensive understanding of this issue is of paramount importance.

In recent years, researchers have explored mathematical models to study unemployment, as documented in various works such as Nikolopoulos and Tzanetis (1999) [15], Misra and Singh (2013) [13], Misra et al. (2017) [14], Pathan and Singh (2017) [16] and Harding (2018) [6]. Initially, Nikolopoulos and Tzanetis (1999) proposed a model, which was further developed by Misra and Singh (2011) to investigate unemployment using three variables. Subsequently, in Misra and Singh (2013), they incorporated time delay and employed the theory of delay differential equations to analyze the model. Building on this concept, Harding and Neamtu (2018) formulated an unemployment model with distributed time delay [6].

Furthermore, prior research in the field has delved into various aspects of three-dimensional unemployment models, encompassing investigations involving discrete time delay [8], distributed time delay [9], and even scenarios with two distinct distributed time delays [18]. In this work is analyzed the model [8] by introducing the optimal control strategy.

These existing mathematical models offer novel approaches to analyze unemployment by leveraging historical data on state variables, which serves as the foundation for the current research work.

²MSC(2010): : 34D23, 91B39, 91B55

Keywords and phrases: *unemployment model, stability properties, optimal control.*

2 The mathematical model

In this study is analyzed the mathematical model of unemployment introduced in [8], incorporating optimal control technique. The paper considers the following aspects:

- Three variables are taken into account: U represents the total number of unemployed individuals, E denotes the total number of employed individuals, and V represents the total number of newly created jobs by the government and private sector.
- The model assumes that all individuals entering the system at time t possess the necessary qualifications for any available job.
- The number of unemployed individuals increases steadily at a constant rate, denoted as A .
- Both the government and private sector exert efforts to generate new job openings, with the number of job opportunities being directly proportional to the number of unemployed individuals.
- It is also assumed that if individuals are fired or voluntarily leave their jobs within the employed group, they transition to the unemployed group.

Based on the previously mentioned considerations, the mathematical model described in [8] is:

$$\begin{cases} \dot{U}(t) = A - [a_1V(t) + a_2]U(t) + a_3E(t) - b_1U(t), \\ \dot{E}(t) = [a_1V(t) + a_2]U(t) - a_3E(t) - b_2E(t), \\ \dot{V}(t) = a_4U(t - \tau) - b_3V(t), \end{cases} \quad (1)$$

with the parameters:

- a_1 - the employment rate pertaining to the newly generated job opportunities by both the government and private sector, specifically aimed at the unemployed individuals;
- a_2 - the employment rate for the unemployed individuals in relation to the existing job positions;
- a_3 - the rate at which individuals transition from the employed category to the unemployed category due to being terminated or voluntarily leaving their jobs;
- b_1 - the death rate and the migration rate of unemployed persons;
- b_2 - the rate of death, retirement and migration of employed persons;
- a_4 - the rate at which new job vacancies are being created;
- b_3 - the diminution of the new vacancies created by government and private sectors;
- τ - discrete time delay

The first result for positivity and boundedness of the solution of the system (1) is proved in [8].

Theorem 2.1. *The set,*

$$\Omega = \left\{ (U, E, V) \in \mathbb{R}^3 : 0 < U + E < \frac{A}{\delta}, 0 < V < \frac{a_4 A}{\delta b_3} \right\},$$

where $\delta = \min(b_1, b_2)$ is a region of attraction for the system (1) and it attracts all the solutions initiating from the interior of the open positive octant of \mathbb{R}^3 .

3 Equilibrium analysis

By solving the system presented as follows:

$$\begin{cases} A - (a_1V + a_2)U + a_3E - b_1U = 0 \\ (a_1V + a_2)U - a_3E - b_2E = 0 \\ a_4U - b_3V = 0 \end{cases} \quad (2)$$

the unique positive equilibrium of the model (1) is determined, which is denoted as S^+ . The equilibrium is given by:

$$S^+ := (U_0, E_0, V_0) = \left(U_0, \frac{U_0(a_1a_4U_0 + a_2b_3)}{b_3(a_3 + b_2)}, \frac{a_4U_0}{b_3} \right).$$

4 Local stability analysis

The characteristic equation for system (1) is:

$$a_1a_4U_0e^{-\lambda\tau}(\lambda + b_2) + \lambda^3 + C_2\lambda^2 + C_1\lambda + C_0 = 0, \quad (3)$$

where the coefficients

$$\begin{aligned} C_2 &= a_1V_0 + a_2 + a_3 + b_1 + b_2 + b_3 \\ C_1 &= a_1b_2V_0 + a_1b_3V_0 + a_2b_3 + a_2b_2 + a_3b_1 + b_1b_2 + b_1b_3 + a_3b_3 + b_2b_3 \\ C_0 &= a_1b_2b_3V_0 + a_2b_2b_3 + b_1b_3a_3 + b_1b_2b_3 \end{aligned}$$

are positive.

Denoting with $P(\lambda) = \lambda^3 + C_2\lambda^2 + C_1\lambda + C_0$, the equation (3) becomes:

$$a_1a_4U_0e^{-\lambda\tau}(\lambda + b_2) + P(\lambda) = 0 \quad (4)$$

In [8], the following results are proven:

Theorem 4.1. *In the non-delayed case, the equilibrium point of the system (1) S^+ is locally asymptotically stable.*

Lemma 4.2. *Considering $\tau > 0$ as bifurcation parameter, system (1) does not undergo a Hopf bifurcation in a neighborhood of the positive equilibrium S^+ , for any value of the time delay.*

The previous lemma implies the following important result:

Theorem 4.3. *The positive equilibrium S^+ of system (1) is locally asymptotically stable for any value of the time delay $\tau \geq 0$.*

5 Optimal control strategy

In this section, the necessary and sufficient condition for the optimal control strategy to be presented is outlined.

Firstly, it is considered t_f and Δ as constants. Then, it is defined an admissible control set $U_{ad} = \{u(t) \text{ which is measurable, } 0 \leq u(t) \leq \Delta, t \in [0, t_f]\}$. The variable $u(t)$ in this context is referred to as a control variable, representing the strategy employed to decrease the number of

unemployed individuals. Based on these facts, it is analyzed an optimal control problem aimed at minimizing the objective functional

$$J(u) = \int_0^{t_f} [U(t) + \frac{\epsilon}{2}u^2(t)]dt \quad (5)$$

under the constraint of:

$$\begin{cases} \dot{U}(t) = A - [a_1V(t) + a_2]U(t) + a_3E(t) - b_1U(t) - u(t)U(t), \\ \dot{E}(t) = [a_1V(t) + a_2]U(t) - a_3E(t) - b_2E(t) + \omega(t)u(t)U(t), \\ \dot{V}(t) = a_4U(t - \tau) - b_3V(t) - \omega(t)u(t)U(t) + u(t)U(t), \end{cases} \quad (6)$$

To ensure a balanced magnitude of the control variable, denoted as $u(t)$, a small positive constant ϵ is introduced. The introduction of this constant accounts for the squared control variable, which signifies the extent of the size effects of the control.

To obtain an optimal solution, the initial step involves deriving the Lagrangian and Hamiltonian for the optimal control problem stated in equations (5) and (6). Specifically, the Lagrangian of the optimal problem can be represented in the following manner:

$$\tilde{L}(U, u) = U(t) + \frac{\epsilon}{2}u^2(t). \quad (7)$$

In order to identify the optimal control function for the provided optimal control problem, we define the corresponding Hamiltonian as follows:

$$H(U, E, V, u, \lambda_1, \lambda_2, \lambda_3, t) = \tilde{L}(U, u) + \lambda_1(t)\dot{U}(t) + \lambda_2(t)\dot{E}(t) + \lambda_3(t)\dot{V}(t), \quad (8)$$

where $\lambda_1, \lambda_2, \lambda_3$ are the adjoint functions to be determined suitably. Firstly, we establish the existence of a solution for the control system (6).

As in [3], we have:

Theorem 5.1. *There exists an optimal control $u^*(t)$ such that $J(u^*(t)) = \min J(u(t))$, under the constraint of the control system stated in (6), along with the given initial conditions.*

Proof. It can be observed:

1. There is a nonempty set of control and corresponding state variables.
2. The admissible set U_{ad} is both convex and closed.
3. The right-hand side of the state system (6) is bounded by a linear function involving the state variables.
4. The function $\tilde{L}(U, u) = U + \frac{\epsilon}{2}u^2$ is concave when considering the admissible control set U_{ad} .
5. There exists a constant $\rho > 1$, $\eta_1 > 0$ and η_2 such that $\tilde{L}(U, u) \geq \eta_1(|u|)^\rho + \eta_2$. Specifically, we can choose $\eta_1 = \frac{\epsilon}{2}$ and η_2 represents the lower bound on U , which is similar to the lower bound mentioned in [7]. Thus, it can be directly obtained the result from [2], completing the proof.

□

Moving forward, a necessary condition for the optimal control strategy is derived using Pontryagin's Maximum Principle [4].

Theorem 5.2. *When considering an optimal control variable $u^*(t)$ and the corresponding solution $U^*(t), E^*(t), V^*(t)$ of state system (6), there exists adjoint variables $\lambda_1(t), \lambda_2(t)$ and $\lambda_3(t)$ that satisfy*

$$\begin{cases} \dot{\lambda}_1(t) = -1 + [a_1V^*(t) + a_2 + b_1 + u^*(t)]\lambda_1(t) - [a_1V^*(t) + a_2 + \omega u^*(t)]\lambda_2(t) - \\ \quad - (1 - \omega)u^*(t)\lambda_3(t) - \chi_{[0, t_f - \tau]}(t)a_4\lambda_3(t + \tau), \\ \dot{\lambda}_2(t) = -a_3\lambda_1(t) + (a_3 + b_2)\lambda_2(t), \\ \dot{\lambda}_3(t) = a_1U^*(t)\lambda_1(t) - a_1U^*(t)\lambda_2(t) + b_3\lambda_3(t), \end{cases} \quad (9)$$

with transversality conditions

$$\lambda_i(t_f) = 0, \quad i = 1, 2, 3.$$

Here $\chi_{[0, t_f - \tau]}(t) = 1$ if $t \in [0, t_f - \tau]$. Otherwise $\chi_{[0, t_f - \tau]}(t) = 0$. Furthermore, the optimal control $u^*(t)$ is given

$$u^*(t) = \min\{\max(0, R), \Delta\}, \quad (10)$$

where

$$R = \frac{U(t+1)}{\epsilon} [\lambda_1(t) - \omega\lambda_2(t) - (1 - \omega)\lambda_3(t)].$$

Proof. To derive the adjoint equations and the transversality conditions, we employ the Hamiltonian stated in equation (8). By differentiating the Hamiltonian (8), we acquire the adjoint system in the following manner:

$$\begin{cases} \dot{\lambda}_1(t) = -\frac{\partial H}{\partial U}(t) - \chi_{[0, t_f - \tau]}(t)\frac{\partial H}{\partial U_\tau}(t + \tau), \\ \dot{\lambda}_2(t) = -\frac{\partial H}{\partial E}(t) - \chi_{[0, t_f - \tau]}(t)\frac{\partial H}{\partial E_\tau}(t + \tau), \\ \dot{\lambda}_3(t) = -\frac{\partial H}{\partial V}(t) - \chi_{[0, t_f - \tau]}(t)\frac{\partial H}{\partial V_\tau}(t + \tau). \end{cases} \quad (11)$$

Hence, the adjoint system can be reformulated as system (9). According to the optimal conditions, we obtain the following:

$$\frac{\partial H}{\partial u}(t)|_{u=u^*(t)} = -\epsilon u^*(t) + \omega\lambda_1(t)V^*(t) + (1 - \omega)\lambda_2(t)V^*(t) - \lambda_3(t)V^*(t) = 0. \quad (12)$$

Consequently, it can be deduced that $u^*(t) = \min\{\max(0, R), \Delta\}$. By considering the characteristics of the admissible control set U_{ad} , equation (10) can be obtained and the proof is finalized.

As a result, we have successfully derived the following optimality system:

$$\begin{cases} \dot{\lambda}_1(t) = -1 + [a_1V^*(t) + a_2 + b_1 + u^*(t)]\lambda_1(t) - [a_1V^*(t) + a_2 + \omega u^*(t)]\lambda_2(t) - \\ \quad - (1 - \omega)u^*(t)\lambda_3(t) - \chi_{[0, t_f - \tau]}(t)a_4\lambda_3(t + \tau), \\ \dot{\lambda}_2(t) = -a_3\lambda_1(t) + (a_3 + b_2)\lambda_2(t), \\ \dot{\lambda}_3(t) = a_1U^*(t)\lambda_1(t) - a_1U^*(t)\lambda_2(t) + b_3\lambda_3(t), \\ u^*(t) = \min\{\max(0, R), \Delta\}, \quad R = \frac{U(t+1)}{\epsilon} [\lambda_1(t) - \omega\lambda_2(t) - (1 - \omega)\lambda_3(t)], \\ \lambda_i(t_f) = 0, \quad i = 1, 2, 3. \end{cases} \quad (13)$$

and

$$\begin{cases} \dot{U}^*(t) = A - [a_1V^*(t) + a_2]U^*(t) + a_3E^*(t) - b_1U^*(t) - u^*(t)U^*(t), \\ \dot{E}^*(t) = [a_1V^*(t) + a_2]U^*(t) - a_3E^*(t) - b_2E^*(t) + \omega(t)u^*(t)U^*(t), \\ \dot{V}^*(t) = a_4U^*(t - \tau) - b_3V^*(t) - \omega(t)u^*(t)U^*(t) + u^*(t)U^*(t). \end{cases} \quad (14)$$

□

6 Numerical simulations

The system parameters for the numerical simulations are as follows: A is chosen as 5000, a_1 is set to 0.00002, a_2 is set to 0.4, a_3 is set to 0.01, a_4 is set to 0.007, $b_1 = 0.04$, $b_2 = 0.05$, $b_3 = 0.05$, $\omega = 0.8$, $\Delta = 0.8$, $\epsilon = 20000$ and $t_f = 500$.

In the initial three instances illustrated in Figure 1, we plotted the evolution of individuals who were unemployed, individuals who were employed, and the number of new jobs generated by both the government and the private sector. These cases included scenarios involving constant high control, optimal control and without control. Based on the findings from Figure 1, it can be concluded that the implemented control measures have proven to be effective.

Figure 2 exhibits the collective evolution of the three variables $U(t)$, $E(t)$, and $V(t)$, alongside the control strategy.

Figure 3 describes the temporal evolution of the state variables $U(t)$, $E(t)$, and $V(t)$ in the absence of the delay and control. Additionally, the figure shows that the equilibrium point of the initial system is asymptotically stable.

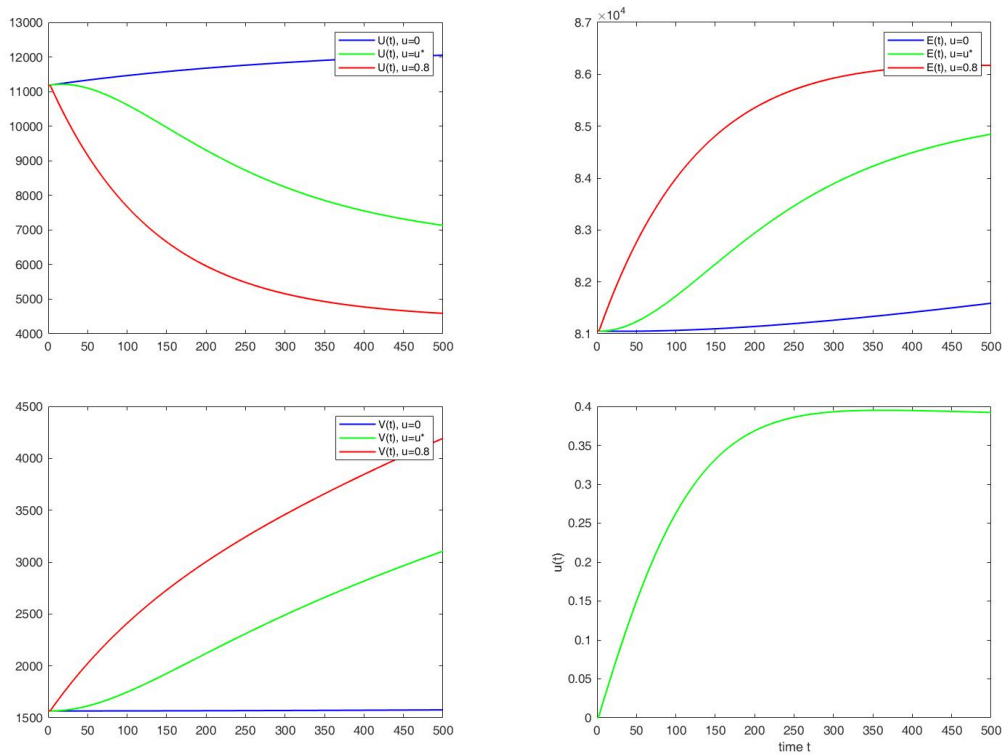


Figure 17: Evolution of state variables $U(t)$, $E(t)$ and $V(t)$ of system (6) with optimal control (red), with high control (red) and without control (blue).

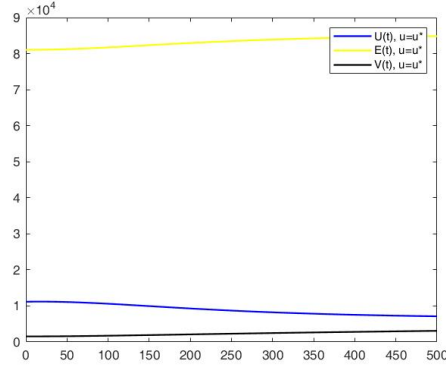


Figure 18: Evolution of state variables $U(t)$ (blue), $E(t)$ (yellow) and $V(t)$ (black) of system (6) with optimal control.

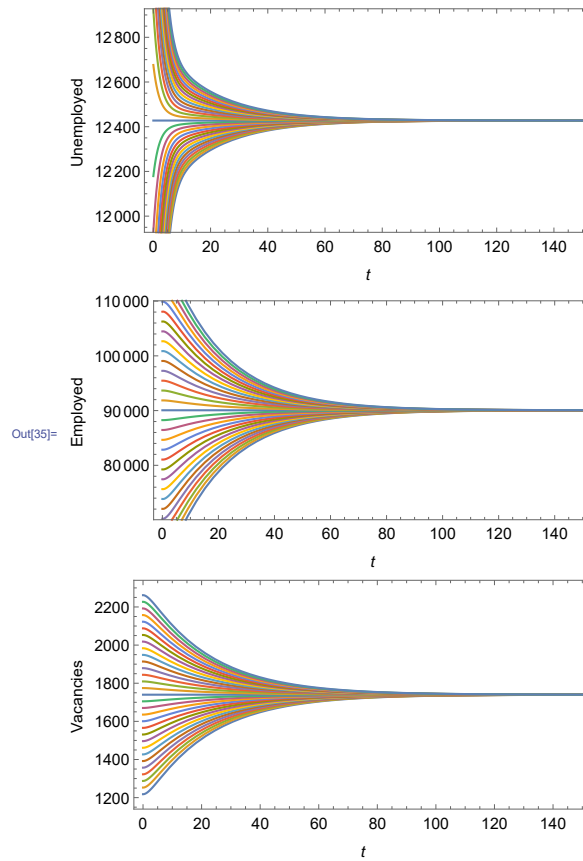


Figure 19: Evolution of state variables $U(t)$, $E(t)$ and $V(t)$ of system (1) without delay and control.

7 Conclusions

In this paper the model proposed in [8] which incorporates one discrete time delay was investigated. Initially, the local stability results were presented, followed by a discussion on the optimal control.

In particular, this work represented the first instance in which an optimal control problem was formulated for the controlled system (1). Theorems 5.1 and 5.2 present an optimal strategy aimed at minimizing the overall count of unemployed individuals.

Furthermore, upon conducting numerical simulations, it becomes evident that it is reasonable to deduce that the control strategy u^* is, indeed, the optimal selection for minimizing the objective function $J(u)$. This study has the potential to provide a fresh outlook on the issue of unemployment control, among other aspects.

Acknowledgement

I would like to express my sincere gratitude to Prof. Dr. Mihaela Neamtu and Prof. Dr. Eva Kaslik for their invaluable support and constructive advice throughout the duration of this academic work.

References

- [1] R. Al-maalwi, H. A. Ashi, S. Al-Sheikh, *Unemployment Model*, Applied Mathematical Sciences, **12(21)** (2018), 989-1006.
- [2] Birkhoff, Garrett *Ordinary differential equations*, 1989.
- [3] Chen, Lijuan and Hattaf, Khalid and Sun, Jitao, *Optimal control of a delayed SLBS computer virus model*, Physica A: Statistical Mechanics and its Applications, (2015), 244-250.
- [4] Flemming, W and RISHEL, RW, *Deterministic and Sochastic Optimal Control Springer-Verlag*, New York, United State of America, 1975.
- [5] J. K. Hale, S. M. V. Lunel, *Introduction to Functional Differential Equations*, Springer Science & Business Media, 2013.
- [6] L. Harding, M. Neamtu, *A dynamic model of unemployment with migration and delayed policy intervention*, Computational Economics, **51(3)** (2018), 427-462.
- [7] Hattaf, Khalid and Yousfi, Noura, *Optimal control of a delayed HIV infection model with immune response using an efficient numerical method*, International Scholarly Research Notices, (2012), 244-250.
- [8] E. Kaslik, M. Neamtu, L. F. Vesa, *An unemployment model with time delay*, Annals of the Academy of Romanian Scientists: Series on Mathematics on its Applications, **12(2020)**, 142-154.
- [9] E. Kaslik, M. Neamtu, L. F. Vesa, *Global stability analysis of an unemployment model with distributed delay*, Mathematics and Computers in Simulation **185** (2021), 535-546.
- [10] E. Kaslik, M. Neamtu, L. F. Vesa, *Global Stability Analysis of a Five-Dimensional Unemployment Model with Distributed Delay*, Mathematics, **9(23)** (2021), 3037.
- [11] V. Kolmanovskii, M. Anatoliy, *Introduction to the theory and applications of functional differential equations*, Springer Science and Business Media, **463** (2013).
- [12] A. K. Misra, Arvind K. Singh, *A mathematical model for unemployment*, Nonlinear Analysis: Real World Applications, **12(1)** (2011), 128-136.
- [13] A. K. Misra, Arvind K. Singh, *A Delay Mathematical Model for the Control of Unemployment*, Differential Equations and Dynamical Systems, **21(3)**(2013), 291-307.

- [14] A.K. Misra, A.K. Singh, P.K. Singh, *Modeling the role of skill development to control unemployment*, Differential Equations and Dynamical Systems, (2017), 1-13.
- [15] C. V. Nikolopoulos, D. E. Tzaneis, *A model for housing allocation of a homeless population due to a natural disaster*, Nonlinear Analysis: Real World Applications, **4** (2003), 561-579.
- [16] G. Pathan, P.H. Bhathawala, *A mathematical model for unemployment-taking an action without delay*, Adv. Dyn. Syst. Appl., **12(1)**, (2017), 41-48.
- [17] H. L. Smith, *An introduction to delay differential equations with applications to the life sciences*, New York: Springer, 2011.
- [18] L. F. Vesa, E. Kaslik, M. Neamțu, *Global Stability Analysis of An Unemployment Model with Two Distributed Time Delays*, Advances in Nonlinear Dynamics. Springer, Cham, (2022), 525-535.

Loredana Flavia VESA – Department of Mathematics,
Politehnica University of Timișoara,
P-ta Victoriei 2, 300 006, Timișoara, ROMANIA
E-mail: loredana.vesa@upt.ro

SOME APPLICATIONS OF MONTE CARLO METHOD IN MEDICINE

Theodora CARTIANU

Abstract

Simulation currently affects our daily lives through our interactions with the automotive industry, airlines, and entertainment. The use of simulation in drug development is relatively new, but its usage is increasing in line with the speed of modern computers. A well-known example of simulation in drug development is molecular modeling. Another use of simulation that has recently been observed in drug development is Monte Carlo simulation in clinical studies. Monte Carlo simulation differs from traditional simulation in that the model parameters are treated as stochastic or random variables rather than fixed values. The purpose of this paper is to provide a brief introduction to Monte Carlo simulation methods.

Computer simulation in the pharmaceutical industry is used in the discovery of new drugs, optimization of chemical processes, and most recently, the design of clinical trials. What most people consider "simulation" are models that build or design physical "things". Examples of this type of simulation include the use of computer-aided design (CAD) technology in designing a commercial product such as a car or an airplane, or molecular modeling of drug-receptor interactions. Often, with this class of simulations, the term "modeling" is used interchangeably, such as molecular modeling. For our purposes, models will be differentiated from simulations in that models are built upon data and look back in time, while simulations are based on models and look forward in time.

3

1 Introduction

The purpose of this paper is not to review those simulations meant to mimic the real world and build physical things, but rather to provide a brief introduction to the class of simulations that

³Mathematical Subject Classification (2020): {62-04, 62P10, 65C05}

Keywords and phrases: Monte Carlo simulation method, modeling, clinical studies

utilize mathematical models of a system, which may include physical processes, events, or decision-making processes, to describe the behavior of the system over long periods of time and incorporate stochastic or random variability into the model. This class of simulation is used for decision-making, understanding complex systems, and solving problems for which there is no closed-form solution. In 1979, the Society for Computer Simulation presented a framework for computer simulations (Fig. 1). In this framework, a problem from the real world is first identified and then converted into a conceptual model, which, for our purposes, will be defined as an abstraction of a real system that contains inputs and outputs, where the inputs of the model are predictive with the observed outputs. Ideally, the model is defined using a mechanistic basis and validated using observational data, but neither is necessarily required. Models have the advantage of allowing a better understanding of processes and systems, enabling the user to manipulate inputs to examine outputs.

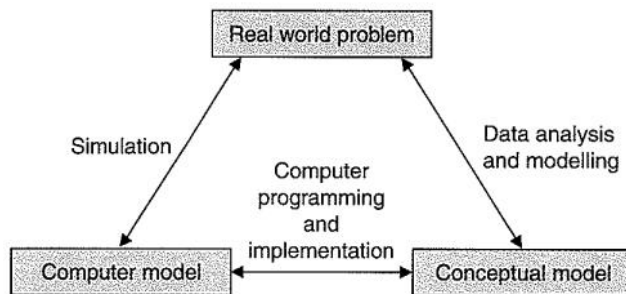


Fig. 1. Framework for computer simulation (modified by the Technical Committee of the Society for Computer Simulation on Model Credibility).

Source: Society for Computer Simulation (SCS) Technical Committee on Model Credibility. Terminology of model credibility. Simulation 1979 Mar: 103-4.

Models and, consequently, simulations can be further classified into discrete event simulations or real-time simulations. Discrete event simulations model a system over time, where variables change instantaneously at certain moments. An example of this is when the occurrence of an adverse reaction happens when plasma concentrations reach a threshold limit. Real-time simulations, which are often observed in clinical trial simulations, model systems where the system changes gradually over time. Of course, some simulations can be a combination of discrete events and real-time processes.

Monte Carlo simulation is the term applied to stochastic simulations, either discrete events, real-time simulations, or a combination thereof, incorporating random variability into the model. The term "Monte Carlo" was first coined by Ulam and von Neumann during World War II and referred to the games of chance in Monaco. The distribution is defined a priori (typically a normal distribution with mean and variance). The Monte Carlo method efficiently simulates the model by repeatedly sampling different random sets of values (inputs) from the parameter sampling distribution, resulting in a set of possible outcomes (outputs).

2 Implementation of Monte Carlo Method in R

Modeling and simulation of clinical studies is a tool used by pharmaceutical companies and the FDA to improve the efficiency of drug development. Monte Carlo Simulation is a modern and computationally efficient algorithm [1]. Therefore, it is a brilliant technique in terms of patient recruitment process and dose calculation in clinical design [2].

The purpose of this paper is to describe how Monte Carlo simulations have the task of evaluating

parameter distributions and their applications in PROC MI.

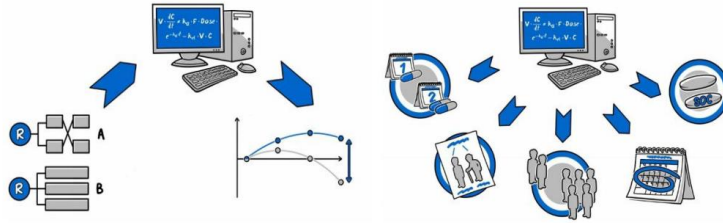


Fig. 2. Clinical Trial Simulation (CTS) explores how different studies design performance to detect the expected effect of the drug. Optimization includes dose regimen, patient profile, sample size, study duration, and the current standard of care (SOC) for patients in the clinical study simulation.

Source: Peter L. Bonate. Clinical Trial Simulation in Drug Development, 2000.

For the univariate data simulation in the data step, we will run R code with the loading of the dataset that can be found at:

<https://archive.ics.uci.edu/ml/machine-learning-databases/00537/>

	A	B	C	D	E	F	G	H	I	J	K	L	M	N	O	P	Q	R	S	T			
1	behavior	set	behavior	aggr	intention	attitude	c	attitude	u_norm	signif	norm	filler	perceptor	perceptor	motivator	motivator	socialSupport	socialSupport	socialSupport	empower	empower	empowerment	ca_cervix
2	10	13	12	4	7	9	10	1	8	7	3	14	8	5	7	12	12	11	8	8	1		
3	10	11	10	14	7	7	5	5	4	2	15	13	7	6	5	5	4	4	4	4	1		
4	10	15	3	2	14	8	10	1	4	7	2	7	3	3	6	11	3	3	15	1			
5	10	11	10	10	15	7	7	1	5	4	2	15	13	7	4	4	4	4	4	1			
6	8	11	7	8	10	7	8	1	5	3	2	15	5	3	6	12	5	4	7	1			
7	10	14	8	6	15	8	10	1	3	4	2	14	8	7	2	7	13	9	6	1			
8	10	15	4	6	14	6	10	5	3	7	2	7	13	3	3	15	3	3	5	1			
9	8	12	9	10	10	5	10	5	5	5	2	10	9	13	2	9	8	7	12	1			
10	10	15	7	2	15	6	10	1	3	5	2	9	15	13	10	15	13	15	15	1			
11	7	15	7	6	11	8	8	5	3	3	4	15	3	8	2	9	3	4	4	1			
12	7	15	7	10	14	7	9	1	3	8	2	4	3	7	9	13	8	3	9	1			
13	10	15	8	9	15	7	10	1	3	7	2	15	3	3	6	13	7	5	9	1			
14	10	15	12	10	15	6	10	1	3	3	2	4	3	3	2	15	13	6	11	1			
15	9	12	14	9	15	10	9	3	6	3	2	15	15	3	10	15	11	3	11	1			
16	2	13	15	6	13	8	9	1	3	3	4	15	3	7	6	7	7	7	3	1			
17	10	15	7	6	14	8	8	4	8	10	2	3	3	3	2	5	5	5	3	1			
18	10	15	9	7	6	8	8	1	12	5	4	5	4	3	3	5	7	7	3	1			
19	10	12	7	5	10	8	8	1	8	10	4	6	3	3	2	4	4	3	5	1			
20	10	11	12	2	10	8	8	2	10	8	7	6	5	3	2	4	4	4	3	1			
21	10	12	12	8	10	8	6	2	7	8	2	12	11	9	8	12	10	10	9	1			
22	10	15	15	4	15	8	10	5	3	8	3	11	3	3	2	7	15	5	3	1			
23	10	12	11	10	15	7	8	3	3	2	13	11	10	7	12	12	12	12	12	0			
24	10	13	14	10	15	6	8	1	5	5	2	15	10	12	8	15	15	15	15	0			
25	10	15	13	10	15	2	10	1	5	6	2	14	14	14	8	14	15	14	15	0			
26	10	12	10	7	15	6	8	2	4	9	2	15	12	10	7	12	14	10	14	0			
27	10	15	13	10	15	6	10	1	3	5	2	15	13	9	7	12	15	11	15	0			
28	10	13	15	8	13	7	8	3	5	9	2	13	11	12	9	10	12	13	12	0			
29	10	15	11	10	15	8	10	1	3	3	2	15	13	13	10	15	15	13	15	0			
30	10	11	11	10	14	5	8	1	4	3	4	15	11	13	9	13	13	12	13	0			
31	10	14	10	9	15	4	5	2	5	7	3	10	7	4	6	7	5	9	12	0			
32	10	14	10	6	15	10	10	1	3	3	7	11	11	11	6	14	15	10	15	0			

```
# load the dataset
sobar_data <- read.csv("C:/Users/LENOVO/Downloads/sobar-72.csv")
# set the parameters for the simulation
N <- 10
NumSamples <- 1000
seed <- 12345
# select variable "self_control" from dataset
x <- sobar_data$self_control
install.packages("dplyr")
install.packages("tidyr")
install.packages("officer")
N <- 10
NumSamples <- 1000
mu <- 5
sigma <- 3
seed <- 12345
Simulation <- data.frame(SampleID = numeric(), x = numeric())
```

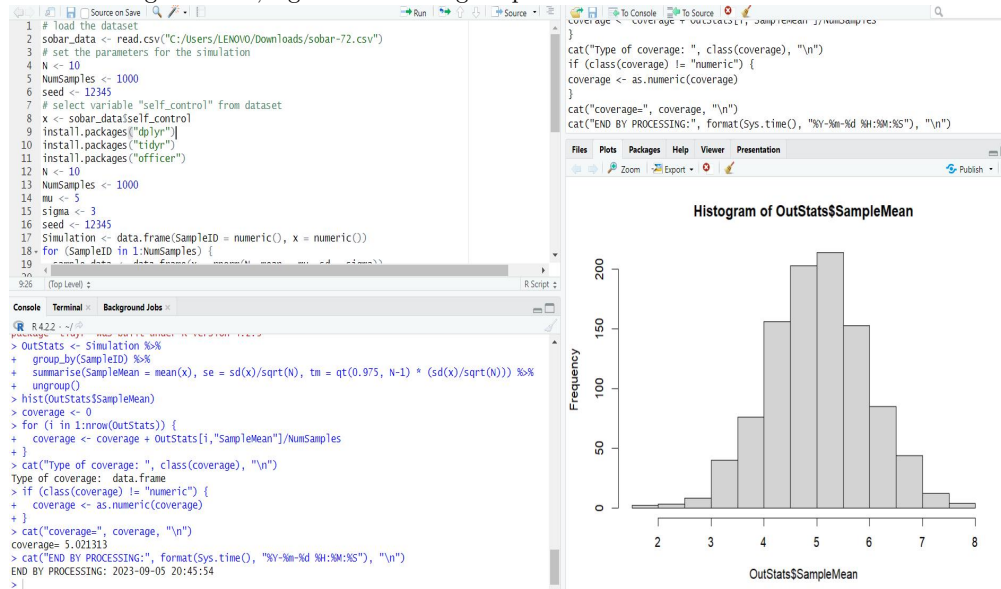


```

for (SampleID in 1:NumSamples) {
  sample_data <- data.frame(x = rnorm(N, mean = mu, sd = sigma))
  sample_data$SampleID <- SampleID
  Simulation <- rbind(Simulation, sample_data)
}
library(dplyr)
library(tidyr)
OutStats <- Simulation %>%
group_by(SampleID) %>%
summarise(SampleMean = mean(x), se = sd(x)/sqrt(N), tm = qt(0.975, N-1) * (sd(x)/sqrt(N)))
%>%
ungroup()
hist(OutStats$SampleMean)
coverage <- 0
for (i in 1:nrow(OutStats)) {
  coverage <- coverage + OutStats[i,"SampleMean"]/NumSamples
}
cat("Type of coverage: ", class(coverage), "\n")
if (class(coverage) != "numeric") {
  coverage <- as.numeric(coverage)
}
cat("coverage=", coverage, "\n")
cat("END BY PROCESSING:", format(Sys.time(), "%Y-%m-%d %H:%M:%S"), "\n")

```

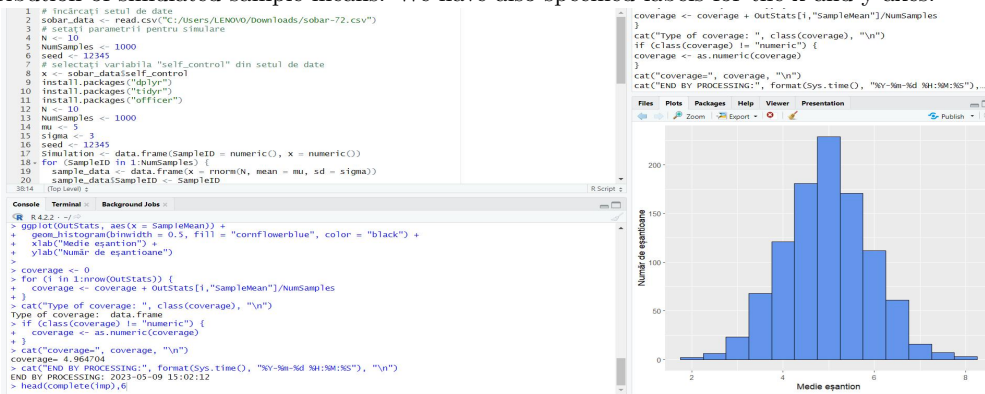
After running the code, I got the following output:



This code aims to perform a simulation of the distribution for the variable "self_control" from a dataset named "sobar-72.csv". Specifically, the code does the following: loads the dataset "sobar-72.csv" using 'read.csv'; sets simulation parameters such as the number of samples ('NumSamples') and the number of observations in each sample ('N'); generates a simulation of a normal distribution with specified mean ('mu') and standard deviation ('sigma') using the 'rnorm' function in a 'for' loop with 'NumSamples' iterations; calculates important statistics for each generated sample, including the mean ('SampleMean'), standard error ('se'), and upper quantile of the 95% confidence interval

(`tm`) using `'group_by'`, `'summarise'`, and `'ungroup'` from the `'dplyr'` package; plots a histogram of the sample means (`'SampleMean'`); calculates the coverage of the 95% confidence interval for the distribution of sample means and displays it using the `'cat'` function; displays the end time of the process using `'format(Sys.time(), "%Y-%m-%d %H:%M:%S")'`.

We obtained a coverage value of approximately 5, which indicates that the 95% confidence interval for the sample mean covers the true mean value with a probability of approximately 95% for each sample. Additionally, we can add the `ggplot2` library and create a histogram plot for the distribution of simulated sample means. We have also specified labels for the x and y axes.



Display the histogram of the sample means distribution

```

ggplot(OutStats, aes(x = SampleMean)) +
  geom_histogram(binwidth = 0.5, fill = "cornflowerblue", color = "black") +
  xlab("Sample Mean") +
  ylab("Number of Samples")

```

Furthermore, I have created a code that creates a Shiny application that allows the user to simulate data based on the chosen distribution and analyze the sensitivity of the simulated results. The user can select the distribution, sample size, and the mu and sigma parameters, and then can view the visualization and results in an interactive table. Furthermore, I have created a code that creates a Shiny application that allows the user to simulate data based on the chosen distribution and analyze the sensitivity of the simulated results. The user can select the distribution, sample size, and the mu and sigma parameters, and then can view the visualization and results in an interactive table.

```

# Install and load required packages
packages <- c("dplyr", "tidyr", "ggplot2", "shiny", "DT", "rmarkdown")
install.packages(packages, dependencies = TRUE)
sapply(packages, library, character.only = TRUE)
# load the dataset
sobar_data <- read.csv("C:/Users/LENOVO/Downloads/sobar-72.csv")
# Define variables for mu and sigma
mu <- 5
sigma <- 3
# set the parameters for the simulation
N <- 10
NumSamples <- 1000
seed <- 12345
# select variable "self_control" from dataset
x <- sobar_data$self_control
# Simulate data with the option to choose the distribution
simulate_data <- function(N, NumSamples, mu, sigma, distribution) {

```

```

Simulation <- data.frame(SampleID = numeric(), x = numeric())
for (SampleID in 1:NumSamples) {
  if (distribution == "normal") {
    sample_data <- data.frame(x = rnorm(N, mean = mu, sd = sigma))
  } else if (distribution == "exponentially") {
    sample_data <- data.frame(x = rexp(N, rate = 1/mu))
  } else if (distribution == "uniform") {
    sample_data <- data.frame(x = runif(N, min = mu - sigma, max = mu + sigma))
  }
  sample_data$SampleID <- SampleID
  Simulation <- rbind(Simulation, sample_data)
}
return(Simulation)
}
# Data validation
validate_data <- function(data) {
  # We can add checks for missing data or outliers here
  # For example: if (any(is.na(data$x))) { ... }
  return(data)
}
# Sensitivity analysis
sensitivity_analysis <- function(N, NumSamples, mu, sigma, distribution) {
  results <- list()
  for (i in 1:10) { # Performs the analysis for 10 sets of parameters
    simulated_data <- simulate_data(N, NumSamples, mu, sigma, distribution)
    validated_data <- validate_data(simulated_data)
    OutStats <- validated_data %>%
      group_by(SampleID) %>%
      summarise(SampleMean = mean(x), se = sd(x)/sqrt(N), tm = qt(0.975, N-1) * (sd(x)/sqrt(N)))
    %>%
    ungroup()
    coverage <- sum(OutStats$SampleMean)/NumSamples
    results[[i]] <- list(params = list(N = N, NumSamples = NumSamples, mu = mu, sigma =
sigma),
      coverage = coverage)
  }
  return(results)
}
# UI for Shiny application
ui <- fluidPage(
  titlePanel("Simulation and Data Analysis"),
  sidebarLayout(
    sidebarPanel(
      selectInput("distribution", " Select Distribution:",
        choices = c("Normal" = "normal", "Exponentially" = "exponential", "Uniform" = "uni-
form")),
      sliderInput("N", " Size Sample:", min = 5, max = 50, value = N),
      numericInput("mu", " Average:", value = mu),
      numericInput("sigma", " Standard Deviation:", value = sigma),
      actionButton("simulateButton", " Simulates")
    ),

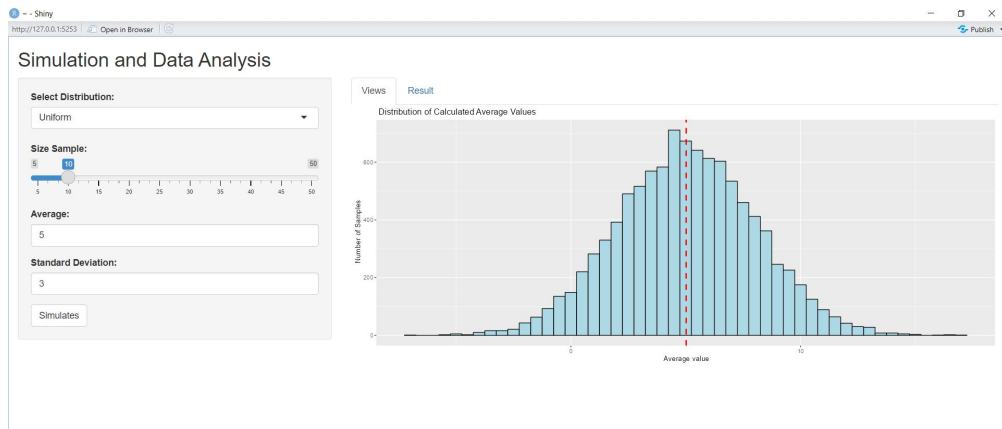
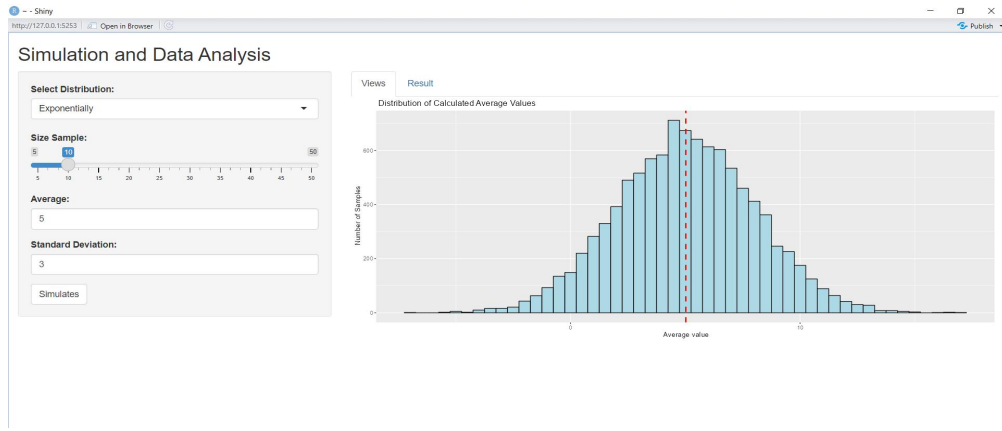
```

```

mainPanel(
  tabsetPanel(
    tabPanel("Views ", plotOutput("histPlot")),
    tabPanel("Result", dataTableOutput("summaryTable"))
  )
)
)
)
)
)
# Server for Shiny application
server <- function(input, output) {
  data <- eventReactive(input$simulateButton, {
    simulate_data(input$N, NumSamples, input$mu, input$sigma, input$distribution)
  })
  output$histPlot <- renderPlot({
    ggplot(data(), aes(x = x)) +
      geom_histogram(binwidth = 0.5, fill = "lightblue", color = "black") +
      geom_vline(aes(xintercept = mean(x)), color = "red", linetype = "dashed", size = 1) +
      labs(title = " Distribution of Calculated Average Values",
           x = " Average value",
           y = " Number of Samples")
  })
  output$summaryTable <- renderDataTable({
    OutStats <- data() %>%
      group_by(SampleID) %>%
      summarise(SampleMean = mean(x), se = sd(x)/sqrt(N), tm = qt(0.975, N-1) * (sd(x)/sqrt(N)))
    %>%
    ungroup()
    datatable(OutStats)
  })
}
# Run the Shiny application
shinyApp(ui = ui, server = server)

```



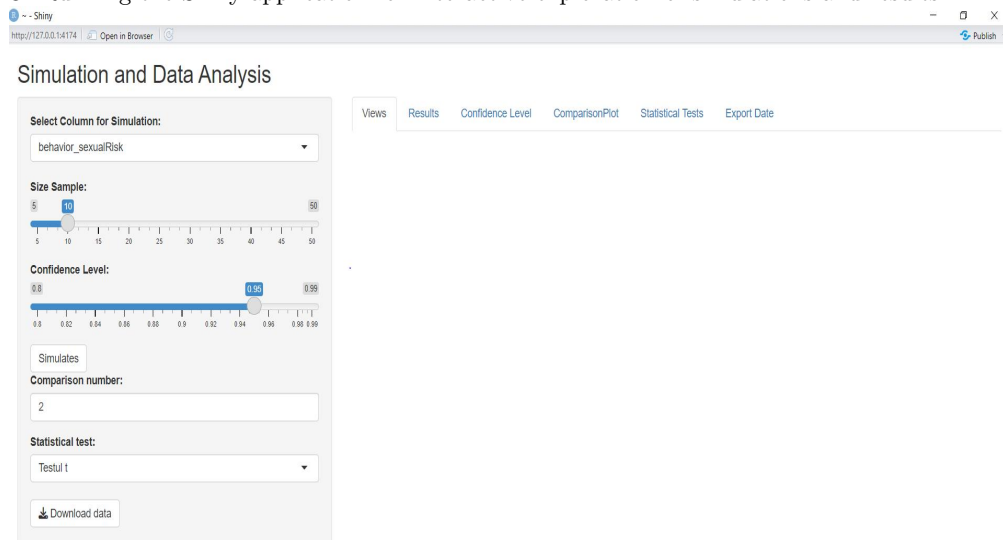


SampleID	SampleMean	se	tm
1	5.187287057500624	1.132729954235405	2.562413179489704
2	4.859266435342303	0.7918761809567618	1.791348374800626
3	4.832813767715709	1.026505792817236	2.32211743187536
4	2.237410998191432	0.9098766840812096	2.058264058157388
5	4.727991121129806	0.9685239473574689	2.19095338485629
6	5.238047537507443	1.126753046397503	2.548892474612809
7	6.398533169008564	1.217440352830626	2.754041414435375
8	6.004497053902774	0.8624055766753783	1.950896952513324
9	4.928232687041284	0.7525935015956415	1.702484780309863
10	7.652797892675146	0.9987947797229454	2.261692922278514

In addition, we can modify the code for the Shiny application in R, following these steps:

1. Installation and loading of necessary packages.

2. Loading a dataset from the "sobrar-72.csv" file and displaying the data.
3. Defining parameters for the simulation, such as mean, standard deviation, and sample size.
4. Simulating data based on the selected column from the dataset.
5. Creating a Shiny interface to allow the user to configure the simulation.
6. Defining a Shiny server that generates visualizations and results, including a histogram, result table, and confidence interval.
7. The ability to compare distributions and perform statistical tests (requires additional implementation).
8. Running the Shiny application for interactive exploration of simulations and results.



3 Missing Data Imputation using The MI Procedure

Missing values pose a problem in a substantial number of clinical analysis studies. Some subjects drop out of the study. Some data is missing due to the patient's illness or death, invalid measurements, or forgetfulness[3]. A statistical analysis can be biased if incomplete cases are excluded from the analysis due to the intent-to-treat (ITT) principle. The MI procedure employs the MCMC method for imputing missing data, simulating the parameters of the model, and diagnosing the model[4].

We will run R code with the loading of the dataset, which can be found at:

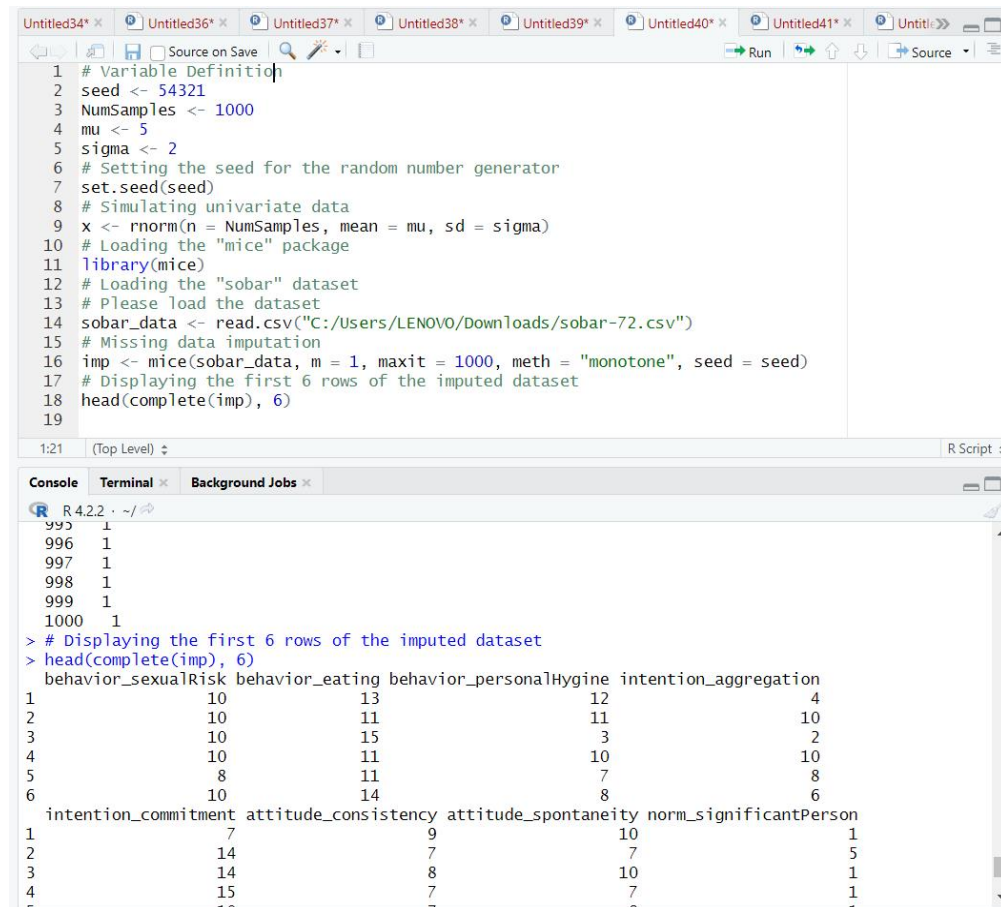
<https://archive.ics.uci.edu/ml/machine-learning-databases/00537/>

```
# Variable Definition
seed <- 54321
NumSamples <- 1000
mu <- 5
sigma <- 2
# Setting the seed for the random number generator
set.seed(seed)
# Simulating univariate data
x <- rnorm(n = NumSamples, mean = mu, sd = sigma)
# Loading the "mice" package
library(mice)
```

```

# Loading the "sobar" dataset
# Please load the dataset
sobar_data <- read.csv("C:/Users/LENOVO/Downloads/sobar-72.csv")
# Missing data imputation
imp <- mice(sobor_data, m = 1, maxit = 1000, meth = "monotone", seed = seed)
# Displaying the first 6 rows of the imputed dataset
head(complete(imp), 6)

```



```

1 # Variable Definition
2 seed <- 54321
3 NumSamples <- 1000
4 mu <- 5
5 sigma <- 2
6 # Setting the seed for the random number generator
7 set.seed(seed)
8 # Simulating univariate data
9 x <- rnorm(n = NumSamples, mean = mu, sd = sigma)
10 # Loading the "mice" package
11 library(mice)
12 # Loading the "sobor" dataset
13 # Please load the dataset
14 sobor_data <- read.csv("C:/Users/LENOVO/Downloads/sobar-72.csv")
15 # Missing data imputation
16 imp <- mice(sobor_data, m = 1, maxit = 1000, meth = "monotone", seed = seed)
17 # Displaying the first 6 rows of the imputed dataset
18 head(complete(imp), 6)
19

```

```

R 4.2.2 ~ /~
995 1
996 1
997 1
998 1
999 1
1000 1
> # Displaying the first 6 rows of the imputed dataset
> head(complete(imp), 6)
  behavior_sexualRisk behavior_eating behavior_personalHygiene intention_aggregation
1             10             13             12             4
2             10             11             11             10
3             10             15             3             2
4             10             11             10             10
5              8             11              7             8
6             10             14              8             6
  intention_commitment attitude_consistency attitude_spontaneity norm_significantPerson
1              7              9              10              1
2             14              7              7              5
3             14              8              10              1
4             15              7              7              1

```

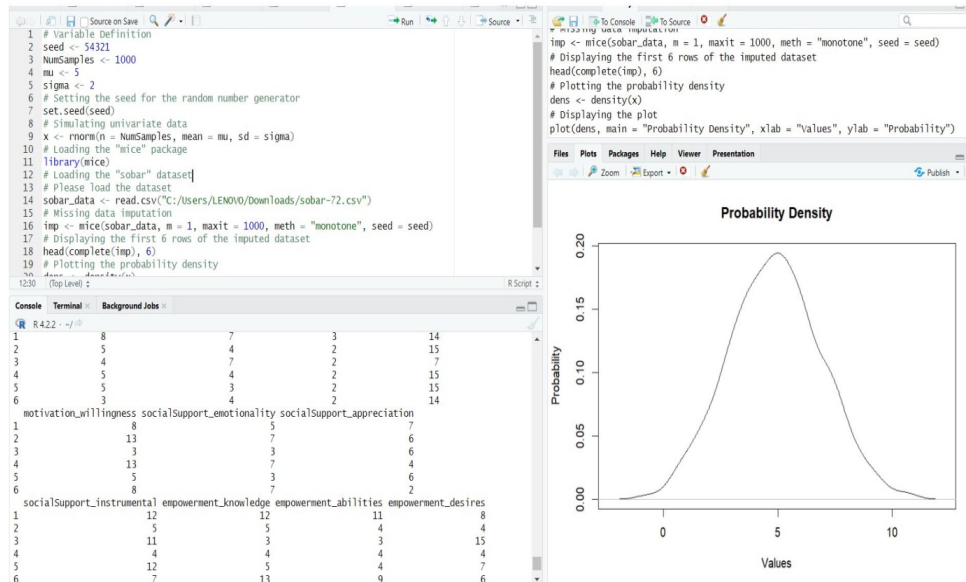
Following the execution of the code, the result will display the first 6 rows of the ‘sobor_data’ dataset with the missing values imputed using the ”monotone” method with the help of the ‘mice’ package. This is achieved by applying the ‘complete()’ function to the ‘imp’ variable, which contains the dataset filled with imputed values.

Additionally, in the above code, we can add plotting the probability density as follows:

```

# Plotting the probability density
dens <- density(x)
# Displaying the plot
plot(dens, main = "Probability Density", xlab = "Values", ylab = "Probability")

```



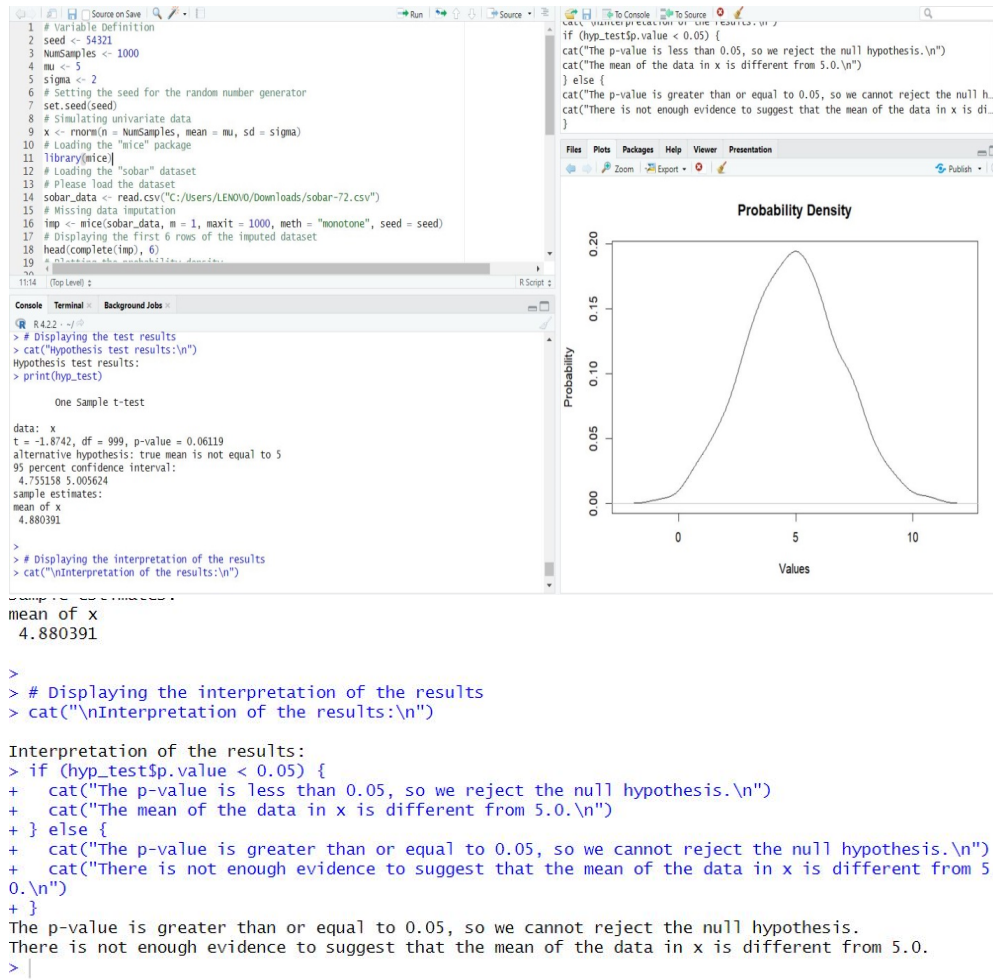
The displayed plot presents the probability density of the values in the 'x' vector. The horizontal axis represents the values in the 'x' vector, while the vertical axis represents the probability density for those values. In this case, the plot shows that the probability density is highest around the value 5, indicating that the values in the 'x' vector are more likely to be closer to this value. Additionally, the probability density is lower around the extreme values, indicating that extreme values are less likely to occur in the 'x' vector.

This code will perform a t-test to check if the mean of the data in x is different from 5.0 and will display the test results along with an interpretation based on the obtained p-value. We can adjust the value of mu and the significance level (0.05 in this example) as needed.

```

# Hypothesis test for the mean of the data in x
hyp_test <- t.test(x, mu = 5)
# Displaying the test results
cat("Hypothesis test results:\n")
print(hyp_test)
# Displaying the interpretation of the results
cat("\nInterpretation of the results:\n")
if (hyp_test$p.value < 0.05) {
  cat("The p-value is less than 0.05, so we reject the null hypothesis.\n")
  cat("The mean of the data in x is different from 5.0.\n")
} else {
  cat("The p-value is greater than or equal to 0.05, so we cannot reject the null hypothesis.\n")
  cat("There is not enough evidence to suggest that the mean of the data in x is different from 5.0.\n")
}

```

4 Conclusions

The Monte Carlo method is a technique used to simulate the behavior of complex systems by generating repeated random values. This method can be used in medicine to estimate the probability of success of a medical procedure, optimize the design and dosage of medications, or evaluate the impact of a new treatment on patients.

Regarding applications in medicine, the Monte Carlo method can be used to simulate treatments and their effects on patients, allowing physicians to better understand the risks and benefits of a particular treatment before administering it to patients. Additionally, this method can be used in the design and testing of new medical devices, such as implants or diagnostic equipment.

Although the Monte Carlo method is very powerful and useful in medicine, there are also some challenges and limitations in its use. For example, in the case of simulating treatments and medical procedures, it can be influenced by individual variations among patients and complex interactions between different elements of the system.

Moreover, solid programming and mathematical modeling expertise are required to successfully implement the Monte Carlo method in medical research.

Therefore, it is important for researchers and physicians to consider these limitations and collaborate with experts in the field of statistical methods and mathematical modeling to achieve the best possible outcomes.

The Monte Carlo method is a powerful and versatile tool in the field of medicine, which can help optimize processes and treatments, reduce risks, and improve the quality of patient care.

However, it is important to consider the limitations of this method and combine it with other methods and technologies to ensure the best possible solution for each specific medical situation.

In conclusion, I would like to thank my supervisor, Associate Professor Dr. Negrea Romeo, as well as my family for all the support they have provided.

References

- [1] Munsaka, Melvin, Using SAS for Modeling and Simulation in Drug Development – A Review and Assessment of Some Available Tools, 2011.
bibitem2 Bonate, Peter L, Clinical Trial Simulation in Drug Development, 2000.
- [2] Wicklin, Rick, SIMULATING DATA with SAS, SAS online document, 2013.
- [3] Patterson, Scott D., SAS Markov Chain Monte Carlo (MCMC) Simulation in Practice, 2007.
vspace-6pt

Theodora CARTIANU
Master student MTSSCC, Politehnica University of Timisoara
Adresa: P-ta victorie 2, 300006, Timisoara, Romania
E-mail:theodora.cartianu@yahoo.com

APPLICATION OF R SOFTWARE TO THE DATA OF THE COMPARATIVE STUDY INTRALESIONAL IMMUNOTHERAPY AND CRYOTHERAPY IN THE TREATMENT OF WARTY LESIONS

Emilia SOUCA

Abstract

For the R software application we have taken two datasets “Immunotherapy” and “Cryotherapy” obtained in comparative study between Intralesional Immunotherapy and Cryotherapy (2) from the database <https://achieve.ics.uci.edu/datasets.php>. This study was conducted in dermatology clinic “Ghaem Hospital”, Mashad, Iran. The study enrolled 180 patients diagnosed with verrucous lesions. The selection of the patients for the application of the treatment method was randomized. The patients were included in two treatment groups in equal number, 90 patients received intralesional immunotherapy treatment with Candida antigen, 90 patients received cryotherapy treatment using liquid nitrogen. In this article the data obtained from this study are analysed as a single dataset by aggregating the two datasets, the study authors analysing them individually. Also the statistical analysis was performed using R software unlike the study authors who performed the analysis using a rule-based fuzzy logic system. The results of the statistical analysis, by evaluating the predicted probabilities, showed that Immunotherapy is more effective than Cryotherapy in treating warty lesions. The values of these probabilities are 0.60 for Cryotherapy treatment and 0.89 for Immunotherapy treatment.

⁴

1 Introduction

Warty lesions are the most common clinical manifestation of human papillomavirus (HPV) infection of the skin and mucous membranes, and are most common on the hands, feet, face and genitals.

⁴Mathematical Subject Classification (2020): {62-04, 62P10, 62J05}

Keywords and phrases: multiple linear regression, Wald test, Akaike’s Informational Criterion

These benign lesions have different clinical forms. Despite the various therapeutic modalities used: topical caustic acid, cryotherapy, electrocautery, surgical removal, laser ablation, intralesional injection of bleomycin, *Candida albicans*, purified protein derivatives; there is still no single method that can be used as an approved treatment(1). Liquid nitrogen cryotherapy is a favourable and alternative treatment, leading to treatment of up 50%– 70% of lesions after three or four session (1). Intralesional immunotherapy is another current treatment that stimulates the immune system to recognise the *Candida* antigen through the delayed hypersensitivity reaction and subsequently eliminate HPV (1).

The clinical study from which these data were obtained was a comparative analysis of intralesional immunotherapy with *Candida* antigen and cryotherapy with liquid nitrogen. The study included 180 patients with common and plantar warty lesions. The two treatment methods represent two of the most effective therapeutic methods. Cryotherapy is the most widely used treatment method. However the presence of side effect and the numerous treatment sessions require to achieve favourable results are not the best option. Immunotherapy is a newer therapeutic method, but it also has the disadvantage found in cryotherapy treatment.

The 180 patients enrolled in the study were divided into two groups. The allocation of patients to the therapeutic variant administered was randomised. The age of the patients ranged from 15 years, the minimum age for inclusion in the study, to 67 years.

	Immunotherapy group	Cryotherapy group
Number of patients	90	90
Age (average)	28.6	31.04
Gender: Male	41	47
Female	49	43
Type of injuries: - <i>Verruca vulgaris</i>	39	49
- Plantar warts	30	19
- Both Types	21	22

Table 1: Demographic characteristics of patients in both groups

Within this dataset, the response variable “Result_of_Treatment” is a binomial type 1 representing the positive response to the treatment applied, and 0 representing the negative response to the treatment applied.

The predictor variables are represented by:

- Variable “age”
- Variable “sex” – categorical variable:
 - 1-male
 - 2- female
- Variable “Time” – time before treatment
- Variable “Number of Warts” – number of warts
- Variable “Type” – type of warty lesions: 1 – *Verruca vulgaris*
 - 2 – Planarian warts
 - 3 – Both types of injuries
- Variable “ Area” – the surface area of warty lesions
- Variable “ Treatment” – type of treatment administered:

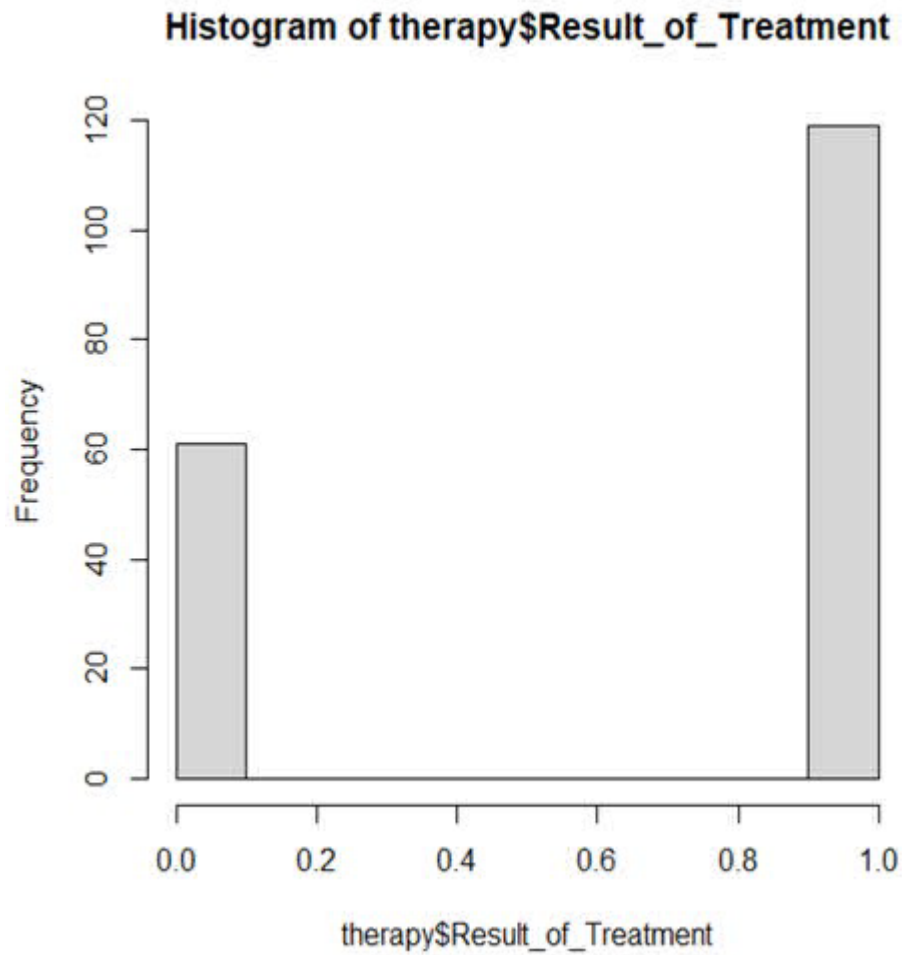


Figure 20: Histogram of the positive/ negative response to treatment

1 – Immunotherapy
0 – Cryotherapy

2 Methods

2.1 Therapeutic methods

Group A received immunotherapy with intralesional injection of Candida antigen, while group B was treated with liquid nitrogen cryotherapy(1). Patient characteristics were recorded in a questionnaire. Warts were assumed to be in the shape of a circle or ellipse(1). To determine the size of the lesions, the two largest perpendicular radii in each lesion were measured in millimetres, and the area was calculated by multiplying the major and minor radii for each lesion, only the area of the largest lesion was calculated(1). Patients were assessed at the beginning of the study, and the number and size of lesions were also noted at each follow-up visit(1). During follow-up, therapeutic response was considered “positive” if the treated lesion area showed a reduction in the size of the largest lesion $>75\%$ (1). A “negative” response was considered when the size reduction was less than 25% of the largest lesion(1). The criteria were applied to both groups. In the case of a partial response (reduction in the size of the largest lesion between 25%- 75%), a negative response was considered(1). Any adverse reactions and their severity were recorded for each patient during the treatment.

Group A

In group A, 0.1 milliliters(ml) of purified Candida 1/1000 antigen solution (Gree USA) was injected intradermally into the flexor side of the left forearm. After 48-72 h, the existence of a response and the size of the skin reaction were assessed. All enrolled patients showed a positive reaction to Candida antigen. The dose of Candida antigen administration for intralesional immunotherapy was determined by the induration diameter after the test dose, as follows: 0.3 ml for an induration diameter of 5-20 mm; 0.2 ml at an induration diameter of 20-40 mm; 0.1 ml for an induration diameter greater than 40 mm. A total of three injections were administrated at 3-week intervals either until the lesions were completely removed or for a maximum of three treatment sessions(1).

Group B

In this group, all patients received cryotherapy once a week until complete elimination of the lesions or for a maximum of 10 sessions. In each session, cryotherapy was done with liquid nitrogen, using cotton probes, until 1-2 mm edge of the normal skin border around the lesion turned white due to frostbite. After thawing, a second cycle was performed in the same way, each session. Any adverse reactions were recorded(1).

2.2 Statistical methods

Model optimization was achieved by applying the GLM function (R package “stats”)(5). The backward method was used for optimization (3). Following the optimization, the important variables for the prediction of the response variable “Result_of_Treatment” are “age”, “Time” and “Treatment”. The Wald test, the Nagelkerke R^2 coefficient, the Brier score and Akaike’s information criterion were used to evaluate the model obtained (3, 4). The values for Related Odds Ratio were calculated for each of the three important predictor variables.

3 Results

3.1 Structure of the optimal model obtained:

Coefficients:

```

Estimate Std. Error z value Pr(>|z|)
(Intercept)
6.48554 1.08357 5.985 2.16e-09 ***
age
-0.07580 0.01802 -4.206 2.60e-05 ***
Time
-0.51240 0.09111 -5.624 1.87e-08 ***
factor(Treatment)1
1.75576 0.45307 3.875 0.000107 ***
---
Signif. codes: 0 '***' 0.001 '**' 0.01 '*' 0.05 '.' 0.1 ' ' 1
(Dispersion parameter for binomial family taken to be 1)
Null deviance: 230.51 on 179 degrees of freedom
Residual deviance: 138.22 on 176 degrees of freedom
AIC: 146.22
Logit( $\pi$ ) =  $\ln\left(\frac{\pi}{1-\pi}\right) = 6.68554 + \text{age} * (-0.07580) + \text{Time} * (-0.51240) + 1.75576 * (\text{Treatment})$ 
> wald.test(b=coef(glm5),Sigma=vcov(glm5),Terms=4)

```

3.2 Wald test

```

-----
Chi-squared test:
X2 = 15.0, df = 1, P(> X2) = 0.00011
A test value of 15.0 was obtained  $\chi^2$  with a degree of freedom associated with P-value of 0.00011
indication that the overall effect of the variable "Treatment" is significant from statistically.

```

3.3 Coefficient Nagelkerke

```

> NagelkerkeR2(glm5)
$N
[1] 180
$R2
[1] 0.5554854
The R2 Nagelkerke Coefficient assessed the explanatory power of a model(4).
Brier score:
> B<-mean((therapy$pred-therapy$Result_of_Treatment)^2)
> B
[1] 0.1111021
> p<-mean(therapy$Result_of_Treatment)
> p
[1] 0.6611111
> Bmax<-p/(1-p)
> Bmax
[1] 1.95082
> Brier<-1-B/Bmax
> Brier
[1] 0.9430485
The Brier score assesses the predictive power of a model(4).

```

3.4 Akaike's Informational Criterion (AIC)

```
> mysteps<-step(glm5,Result_of_Treatment~age+Time+factor(Treatment),family=
  binomial,data=therapy)
  Start: AIC=146.22
  Result_of_Treatment ~ age + Time + factor(Treatment)
  Df Deviance AIC
  <none> 138.22 146.22
  - factor(Treatment) 1 155.27 161.27
  - age 1 158.76 164.76
  - Time 1 188.04 194.04
```

3.5 Odds Ratio

```
exp(cbind(OR=coef(glm5),confint(glm5)))
  ||@ |p() * 1.0000@
-----
  OR 2.5 % 97.5 %
  (Intercept)
  655.5905125 95.3649233 6888.5416219
  age
  0.9270006 0.8930832 0.9589752
  Time
  0.5990590 0.4932874 0.7068576
  factor(Treatment)1
  5.7878504 2.4582063 14.6789690
```

3.6 Predicted probabilities by therapeutic option

```
> head(newdata1)
  age Time Treatment TreatmentP
  1 29.82222 7.448611 0 0.6006916
  2 29.82222 7.448611 1 0.8969798
```

4 Conclusions

Applying the Wald Test (R package “aod”), a value of 15.0 was obtained for the χ^2 with a degree of freedom, associated with a P-value of 0.00011 which shows that the overall effect of the variable “Treatment” is statistically significant. The R^2 Nagelkerke Coefficient value is 0.555 (R package “fmsb”), showing the strenght of the model in explaining the response variable. The adjusted Brier score obtained 0.94, shows the predictive power of the model. By applying the step function (R package “lmerTest”) it was observed that the value of the deviance and AIC increased in the situation of removing the predictor variables from the obtained optimal model.

Since the confidence intervals for the Odds Ratio (OR) obtained by processing in R did not include the value 1, it can be stated that for an increase of one unit (one year) in the variable “age” the patients’ odds will be modified by a factor of 0.92 (decrease); for an increase of one unit (one month) in the variable “Time” the patients’ odds will be modified by a factor of 0.599 (decrease). Since the variable “Treatment” is a categorial variable, the reference category being Cryotherapy for a chance ratio=5.78, the chances of a patients treated with Immunotherapy are changed by a factor equal to this ratio (5.78) compare to the chances of the patients treated with Cryotherapy.

The predicted probabilities obtained, with the variables “age” and “time” held constant (mean), are 0.60 for the Cryotherapy treatment and 0.89 for the Immunotherapy treatment. The interpretation of these results is: a patient aged 29.82 years (mean age) with a time of 7.45 months (mean) before treatment for which the therapeutic option is Cryotherapy has a probability of a positive response to treatment of 0.60; a patient with Immunotherapy treatment has a probability of a positive response of 0.89. For an easier representation of the predicted probabilities according to the type of treatment, age and time prior to treatment administration, the graphical method (R package “ggplot”) (5) was also used.

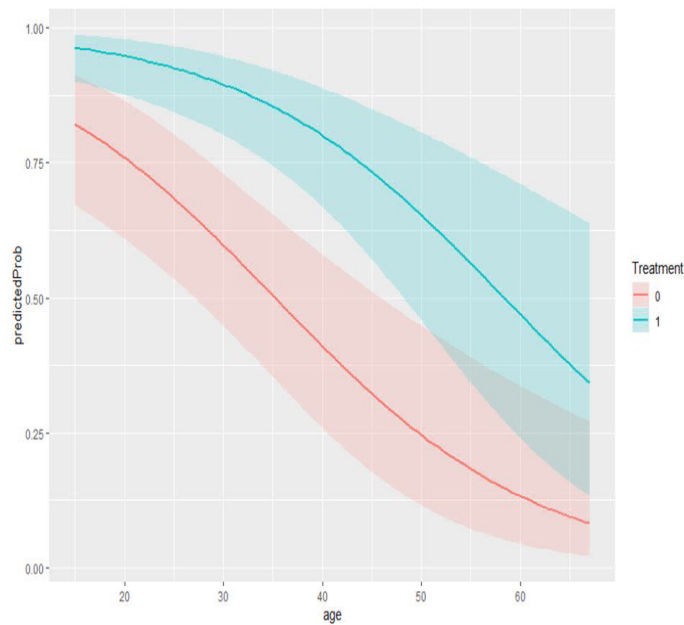


Fig. 2. Predicted probabilities by treatment type and age

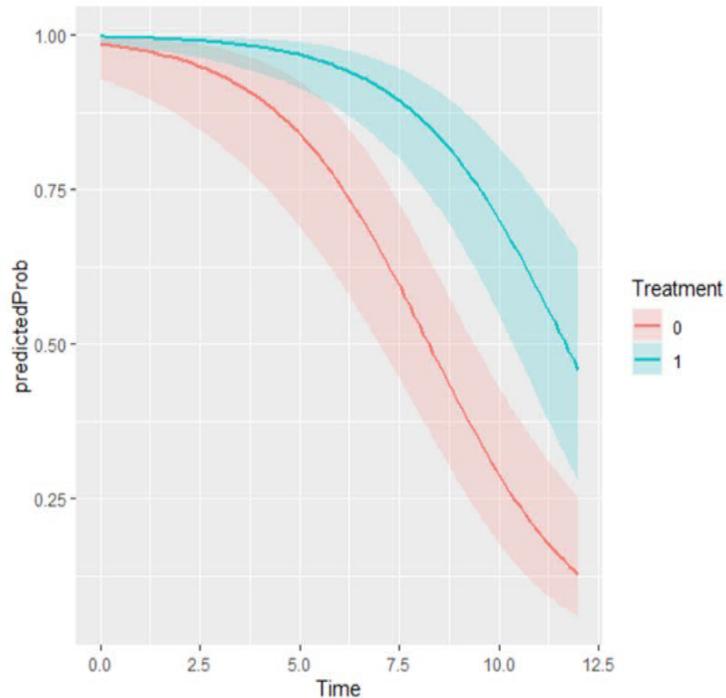


Fig 3. Predicted probabilities by treatment type and time to treatment

Following the statistical analysis, it can be stated that for the dataset presented, age has a negative effect on treatment response for both treatment options: immunotherapy and cryotherapy. Increasing the age of the patients leads to a decrease in the probability of cure. The same influence is also seen in the length of time prior to the treatment with a negative effect on treatment response, increasing it decreases the probability of cure. In terms of type of treatment, Immunotherapy has been shown to be more effective than Cryotherapy in treating warty lesions.

Khozeimeh F. et al performed statistical analysis of the data using a rule-based fuzzy logic system. They found a better therapeutic effect of Immunotherapy compare to Cryotherapy and the presence of a correlation between age and treatment response, but only in the Cryotherapy group. Patients under 21 years of age showed a better response to cryotherapy treatment. Treatment groups were evaluated individually. There was no mention of a relationship between time prior to treatment and treatment response.

Consulting a dermatology specialist from Timisoara Dermatology Clinic confirmed the results obtained by running the dataset in R.

Increasing age decreases the positive response to treatment. The time between the onset of the symptoms and the administration of treatment negatively influences the response to treatment because the lesion becomes deeper and more extensive with the passage of time. Intralesional immunotherapy is more effective than cryotherapy because cryotherapy treatment only removes the surface lesion without treating the human papillomavirus infection.

References

- [1] F. Khozeimeh, R. Alizadehsani, M. Roshanzamir, A. Khosravi, P. Layegh, and S. Nahavandi, An expert system for selecting wart treatment method, *Computers in Biology and Medicine*, vol. 81, pp. 167-175, 2/1/ 2017.
- [2] <https://achieve.ics.uci.edu/datasets.php>
- [3] R. Negrea, *Generalized Linear Models Courses*, Polytechnic University of Timisoara, electronic lectures.
- [4] B. North, F. Gordon, R. Horhat, I. Iercan, *Introduction to Diagnostic Tests and Prognostic Models using R*, London, Imperial College, stathelp@ic.ac.uk, www.imperial.ac.uk/stathelp
- [5] R Core Team (2022). *R: A language and environment for statistical computing*. R Foundation for Statistical Computing, Vienna, Austria, URL <https://www.R-project.org/>.
vspace-6pt

Emilia SOUCA (CRASOVAN)
Master student MTSSCC, Politehnica University of Timisoara
Adresa: P-ta victorie 2, 300006, Timisoara, Romania
E-mail:emiliacrasovan3@gmail.com

SPECTRAL MAPPING THEOREM FOR GENERALIZED EVOLUTION SEMIGROUPS

Nicolae LUPA

Abstract

In the paper [N. Lupa, L. H. Popescu, *Generalized evolution semigroups and general dichotomies*, Results Math. 78 (2023): 112] the authors introduced a special class of real semiflows in order to associate evolution semigroups to not necessarily exponentially bounded evolution families, called as *generalized evolution semigroups*. We give a direct proof of the spectral mapping theorem for generalized evolution semigroups. ⁵

1 Introduction

The theory of evolution semigroups has a significant importance in the study of the asymptotic behavior of their underlying evolution families. For instance, the exponential dichotomy of an evolution family is equivalent to the hyperbolicity of its corresponding evolution semigroup (see [4, Theorem VI.9.18]). The key to the proof lies in the spectral mapping theorem: *the evolution semigroup $\{T_t\}_{t \geq 0}$ corresponding to an exponentially bounded evolution family satisfies the spectral mapping formula*

$$\sigma(T_t) \setminus \{0\} = e^{t\sigma(G)}, t \geq 0,$$

where G is the generator of the semigroup $\{T_t\}_{t \geq 0}$. However, the classical theory of evolution semigroups is too restrictive since it is only addresses to *exponentially bounded* evolution families.

In [5] the authors successfully constructed a framework for a generalization of the concept of evolution semigroups associated to not necessarily exponentially bounded evolution families in order to characterize a wide class of dichotomies, which can occur naturally for instance when all Lyapunov exponents are infinite or they are all zero [2].

More precisely, it is proved that any non-degenerate real semiflow $\varphi : \mathbb{R}_+ \times \mathbb{R} \rightarrow \mathbb{R}$ is determined by a continuous strictly increasing function $\mu : \mathbb{R} \rightarrow \mathbb{R}$ such that $\mu(s) \rightarrow -\infty$ as $s \rightarrow -\infty$ and

$$\varphi(t, s) = \mu^{-1}(\mu(s) - t), \text{ for all } t \geq 0 \text{ and } s \in \mathbb{R}$$

[5, Theorem 2.5]. We recall that a *non-degenerate real semiflow* is a continuous function $\varphi : \mathbb{R}_+ \times \mathbb{R} \rightarrow \mathbb{R}$ satisfying the following properties:

⁵MSC(2010): 47D06, 34G10

Keywords and phrases: *Evolution families, evolution semigroups, spectral mapping theorem.*

- $\varphi(0, s) = s, s \in \mathbb{R}$;
- $\varphi(t, \varphi(\tau, s)) = \varphi(t + \tau, s), t, \tau \geq 0, s \in \mathbb{R}$;
- $\varphi(t, s) \leq s, t \geq 0, s \in \mathbb{R}$;
- any orbit $o(s) = \{\varphi(t, s) : t \geq 0\}$ is non-trivial, i.e. $o(s) \neq \{s\}$.

Furthermore, it is proved that any non-degenerate real semiflow $\varphi : \mathbb{R}_+ \times \mathbb{R} \rightarrow \mathbb{R}$ with

$$\lim_{s \rightarrow \infty} \varphi(t, s) = +\infty, \text{ for } t \geq 0,$$

that is $\mu(s) \rightarrow \infty$ as $s \rightarrow \infty$, and any evolution family $\{U(t, \tau)\}_{t \geq \tau}$ satisfying the inequality

$$\|U(s, \varphi_t(s))\| \leq Ke^{\alpha t}, t \geq 0, s \in \mathbb{R},$$

for some constants $\alpha > 0$ and $K \geq 1$, which is equivalent to

$$\|U(t, \tau)\| \leq Ke^{\alpha(\mu(t) - \mu(\tau))}, t \geq \tau, \quad (1)$$

define a strongly continuous semigroup $\{T_t\}_{t \geq 0}$ on $C_0(\mathbb{R}, E)$ by

$$T_t u(s) = U(s, \varphi_t(s))u(\varphi_t(s)) = U(s, \mu^{-1}(\mu(s) - t))u(\mu^{-1}(\mu(s) - t)), \quad (2)$$

called as *generalized evolution semigroup* (see [5, Theorem 3.3]). Remark that if we consider in (2) the right translation semiflow $\varphi(t, s) = s - t$, which means that $\mu(s) = s$, we step over the classical concept of the evolution semigroup,

$$T_t u(s) = U(s, s - t)u(s - t), t \geq 0, u \in C_0(\mathbb{R}, E), s \in \mathbb{R}.$$

Using the fact that the generalized evolution semigroup is similar to the classical evolution semigroup (see Sect. 3.2 in [5]) one can easily established the spectral mapping theorem in this context.

The aim of this note is to give a direct proof of the spectral mapping theorem for the generalized evolution semigroup introduced in [5], without using the similarity relation mentioned above.

2 Generalized evolution semigroups

Let E be a complex Banach space and let $\mathcal{B}(E)$ be the Banach algebra of all bounded linear operators on E . To simplify notations both norms on E and on $\mathcal{B}(E)$ are denoted by $\|\cdot\|$. Moreover, $C(\mathbb{R}, E)$ is the space of all continuous functions $u : \mathbb{R} \rightarrow E$ and $C_0(\mathbb{R}, E)$ denotes the Banach space of all functions in $C(\mathbb{R}, E)$ vanishing at $\pm\infty$, that is

$$C_0(\mathbb{R}, E) = \left\{ u \in C(\mathbb{R}, E) : \lim_{|s| \rightarrow \infty} u(s) = 0 \right\},$$

endowed with the sup-norm

$$\|u\|_\infty = \sup_{s \in \mathbb{R}} \|u(s)\|.$$

It is well-known that $C_c(\mathbb{R}, E) = \{u \in C(\mathbb{R}, E) : \text{supp}(u) \text{ is compact}\}$ is dense in $C_0(\mathbb{R}, E)$.

A collection $\mathcal{U} = \{U(t, \tau)\}_{t \geq \tau}$ of bounded linear operators $U(t, \tau)$ on E is called an *evolution family* (on the real line) on E if:

- $U(t, t) = I, t \in \mathbb{R}$, here I denotes the identity on E ;
- $U(t, \tau)U(\tau, t_0) = U(t, t_0), t \geq \tau \geq t_0$ in \mathbb{R} ;
- for each $x \in E$, the mapping $(t, \tau) \mapsto U(t, \tau)x$ is continuous on

$$\Delta = \{(t, \tau) \in \mathbb{R}^2 : t \geq \tau\}.$$

It is known that if \mathcal{U} is *exponentially bounded*, i.e. there exist two real constants $\alpha > 0$ and $K \geq 1$ such that

$$\|U(t, \tau)\| \leq Ke^{\alpha(t-\tau)}, \quad t \geq \tau, \quad (3)$$

then one can define a strongly continuous semigroup on $X = C_0(\mathbb{R}, E)$ by

$$T_t u(s) = U(s, s-t)u(s-t), \quad t \geq 0, \quad u \in C_0(\mathbb{R}, E), \quad s \in \mathbb{R},$$

called *the evolution semigroup* associated to \mathcal{U} (see, for instance, [4, Lemma VI.9.10] or [3, Proposition 3.11]). The above concept of evolution semigroup was extended by Råbiger and Schnaubelt to a large class of E -valued function spaces, including in particular the space $C_0(\mathbb{R}, E)$ [6].

We recall that a *strongly continuous semigroup* or a C_0 -*semigroup* on a Banach space X is a family $\{T_t\}_{t \geq 0}$ of operators in $\mathcal{B}(X)$ satisfying:

- $T_0 = I$;
- $T_t T_\tau = T_{t+\tau}$, for $t, \tau \geq 0$;
- $T_t x \rightarrow x$ in X as $t \rightarrow 0^+$ for every fixed $x \in X$.

The (infinitesimal) *generator* of a strongly continuous semigroup $\{T_t\}_{t \geq 0}$ is the linear operator G , with domain $D(G)$, defined by

$$D(G) = \left\{ x \in X : \lim_{t \rightarrow 0^+} \frac{T_t x - x}{t} \text{ exists} \right\}$$

and

$$Gx = \lim_{t \rightarrow 0^+} \frac{T_t x - x}{t}, \quad x \in D(G).$$

We refer the reader to the monograph of Engel and Nagel [4] for a brief history of strongly continuous semigroups.

Let $\mu : \mathbb{R} \rightarrow \mathbb{R}$ be a continuous strictly increasing function such that

$$\lim_{s \rightarrow -\infty} \mu(s) = -\infty \quad \text{and} \quad \lim_{s \rightarrow +\infty} \mu(s) = +\infty,$$

and let \mathcal{U} be an evolution family satisfying (1), which is a natural generalization of the condition (3).

From [5, Theorem 3.3] we get that the family $\{T_t\}_{t \geq 0}$ defined by Eq. (2) is a C_0 -semigroup on $C_0(\mathbb{R}, E)$, called the *generalized evolution semigroup* associated to μ and \mathcal{U} . In the following, we denote by G the generator of the generalized evolution semigroup.

[Rescaled generalized evolution semigroup] It is easy to check that for any $\lambda \in \mathbb{C}$ the evolution family

$$V(t, s) = e^{-\lambda(\mu(t) - \mu(s))} U(t, s), \quad t \geq s,$$

satisfies the inequality

$$\|V(t, s)\| \leq Ke^{(\alpha + |\lambda|)(\mu(t) - \mu(s))}, \quad t \geq s,$$

and thus one can define its generalized evolution semigroup $\{T_t^\lambda\}_{t \geq 0}$ on $C_0(\mathbb{R}, E)$ with respect to μ . More precisely, T_t^λ is given by

$$T_t^\lambda = e^{-\lambda t} T_t, \quad t \geq 0,$$

where $\{T_t\}_{t \geq 0}$ is the generalized evolution semigroup associated to μ and \mathcal{U} .

Furthermore, the generator of $\{T_t^\lambda\}_{t \geq 0}$ is $G - \lambda I$ and its spectrum is given by

$$\sigma(G - \lambda I) = \sigma(G) - \lambda.$$

3 Spectral mapping theorem

We are now able to generalize the spectral mapping theorem for generalized evolution semigroups. Let us first recall some basic notions and results from the spectral theory.

Let $(A, D(A))$ be a closed operator on the Banach space E . A complex number $\lambda \in \mathbb{C}$ belongs to *the residual spectrum* $R\sigma(A)$ if the set $(\lambda I - A)D(A)$ is not dense in E and belongs to *the approximate point spectrum* $A\sigma(A)$ if there exists a sequence $(x_n)_{n \in \mathbb{N}}$ in $D(A)$ with $\|x_n\| \geq 1$ such that $(\lambda I - A)x_n \rightarrow 0$.

It is well-known that any C_0 -semigroup $\{T_t\}_{t \geq 0}$ with the generator $(A, D(A))$ satisfies the spectral inclusion relation

$$e^{t\sigma(A)} \subset \sigma(T_t), \quad t \geq 0. \quad (4)$$

Furthermore, the residual spectra of the semigroup and its generator satisfy

$$e^{tR\sigma(A)} = R\sigma(T_t) \setminus \{0\}, \quad t \geq 0. \quad (5)$$

Theorem 3.1 (Spectral mapping theorem). *The generalized evolution semigroup $\{T_t\}_{t \geq 0}$ satisfies the spectral mapping formula*

$$\sigma(T_t) \setminus \{0\} = e^{t\sigma(G)}, \quad t \geq 0. \quad (6)$$

Proof. We adjust the arguments in [6, Theorem 2.3] for our purpose. Since

$$\sigma(T_t) = R\sigma(T_t) \cup A\sigma(T_t),$$

by (4) and (5) it suffices to prove that

$$A\sigma(T_t) \setminus \{0\} \subset e^{t\sigma(G)}, \quad t \geq 0.$$

In fact, this inclusion is a consequence of a weaker assertion:

$$1 \in A\sigma(T_{t_0}) \text{ for some } t_0 > 0 \text{ implies } 0 \in \sigma(G). \quad (7)$$

Indeed, if $z \in A\sigma(T_{t_0}) \setminus \{0\}$, then $1 \in A\sigma(e^{-\lambda t_0} T_{t_0})$, where $z = e^{\lambda t_0}$. Applying (7) for the C_0 -semigroup $\{e^{-\lambda t_0} T_{t_0}\}$ and using the results in Example 2, we get that $0 \in \sigma(G) - \lambda$. This yields $\lambda \in \sigma(G)$ and thus $z \in e^{t_0 \sigma(G)}$.

It remains to prove (7). Assume that $1 \in A\sigma(T_{t_0})$ for some $t_0 > 0$. Then there exists a sequence (u_n) in $C_0(\mathbb{R}, E)$ such that $\|u_n\|_\infty = 1$ for all $n \in \mathbb{N}$ and

$$\|T_{t_0} u_n - u_n\|_\infty \rightarrow 0.$$

From the inequality

$$\|T_{kt_0} u_n - u_n\|_\infty \leq \left(1 + \|T_{t_0}\| + \cdots + \|T_{t_0}\|^{k-1}\right) \|T_{t_0} u_n - u_n\|_\infty, \quad k \in \mathbb{N}^*,$$

we get that for each $n \in \mathbb{N}$ there exists $k_n \in \mathbb{N}$ such that

$$\|T_{kt_0} u_{k_n} - u_{k_n}\|_\infty < \frac{1}{2}, \quad \text{for } k = \overline{0, 2n}.$$

Therefore,

$$\frac{1}{2} < \|T_{kt_0} u_{k_n}\|_\infty < \frac{3}{2}, \quad \text{for } k = \overline{0, 2n},$$

which is equivalent to

$$\frac{1}{2} < \sup_{s \in \mathbb{R}} \|U(s, \mu^{-1}(\mu(s) - kt_0)) u_{k_n}(\mu^{-1}(\mu(s) - kt_0))\| < \frac{3}{2}, \quad \text{for } k = \overline{0, 2n}. \quad (8)$$

The left-hand side of the above inequality implies

$$\sup_{s \in \mathbb{R}} \|U(s, \mu^{-1}(\mu(s) - nt_0))u_{k_n}(\mu^{-1}(\mu(s) - nt_0))\| > \frac{1}{2}.$$

For each $n \in \mathbb{N}$ take $s_n \in \mathbb{R}$ such that

$$\|U(s_n, \mu^{-1}(\mu(s_n) - nt_0))x_n\| > \frac{1}{2}, \quad (9)$$

where $x_n = u_{k_n}(\mu^{-1}(\mu(s_n) - nt_0))$.

For each $n \in \mathbb{N}^*$ put $I_n = [\mu(s_n) - nt_0, \mu(s_n) + nt_0]$ and pick a continuously differentiable function $\alpha_n : \mathbb{R} \rightarrow \mathbb{R}$ such that

$$\alpha_n(\mu(s_n)) = 1, \quad 0 \leq \alpha_n \leq 1, \quad \text{supp}(\alpha_n) \subset I_n,$$

and

$$|\alpha_n'(\mu(s))| \leq \frac{2}{nt_0}, \quad \text{for every } s \in \mathbb{R}.$$

Let us now define a function $v_n : \mathbb{R} \rightarrow E$ by

$$v_n(s) = \begin{cases} \alpha_n(\mu(s))U(s, \mu^{-1}(\mu(s_n) - nt_0))x_n, & s \geq \mu^{-1}(\mu(s_n) - nt_0), \\ 0, & \text{otherwise.} \end{cases}$$

One can easily check that $v_n \in C_c(\mathbb{R}, E)$ and $\text{supp}(v_n) \subset \mu^{-1}(I_n)$.

Furthermore, from (9) we get

$$\|v_n\|_\infty \geq \|v_n(s_n)\| = \|U(s_n, \mu^{-1}(\mu(s_n) - nt_0))x_n\| > \frac{1}{2}.$$

For $s \geq \mu^{-1}(\mu(s_n) + t - nt_0)$ we have

$$T_t v_n(s) = \alpha_n(\mu(s) - t)U(s, \mu^{-1}(\mu(s_n) - nt_0))x_n,$$

thus

$$\frac{1}{t}(T_t v_n - v_n)(s) = \frac{1}{t}(\alpha_n(\mu(s) - t) - \alpha_n(\mu(s)))U(s, \mu^{-1}(\mu(s_n) - nt_0))x_n.$$

This yields that $v_n \in D(G)$ and

$$Gv_n(s) = \begin{cases} -\alpha_n'(\mu(s))U(s, \mu^{-1}(\mu(s_n) - nt_0))x_n, & s \geq \mu^{-1}(\mu(s_n) - nt_0), \\ 0, & \text{otherwise.} \end{cases}$$

Fix $s \in \mu^{-1}(I_n)$ and put $k = \left\lceil \frac{\mu(s) - \mu(s_n)}{t_0} \right\rceil + n$. It follows that $k \in \{0, 1, \dots, 2n\}$. Moreover, writing

$$\frac{\mu(s) - \mu(s_n)}{t_0} = \left\lfloor \frac{\mu(s) - \mu(s_n)}{t_0} \right\rfloor + c_s, \quad \text{with } c_s \in [0, 1),$$

we get

$$s = \mu^{-1}(\mu(s_n) + (k - n)t_0 + c_s t_0).$$

Using (1) and the right-hand side of (8) we have

$$\begin{aligned} \|Gv_n(s)\| &\leq \frac{2}{nt_0} \|U(s, \mu^{-1}(\mu(s_n) - nt_0))x_n\| \\ &= \frac{2}{nt_0} \|U(\mu^{-1}(\mu(s_n) + (k - n)t_0 + c_s t_0), \mu^{-1}(\mu(s_n) - nt_0))x_n\| \\ &\leq \frac{2}{nt_0} K e^{\alpha c_s t_0} \|U(\mu^{-1}(\mu(s_n) + (k - n)t_0), \mu^{-1}(\mu(s_n) - nt_0))x_n\| \\ &\leq \frac{2}{nt_0} K e^{\alpha t_0} \|U(\mu^{-1}(\mu(s_n) + (k - n)t_0), \mu^{-1}(\mu(s_n) + (k - n)t_0 - kt_0))x_n\| \\ &\leq \frac{3}{nt_0} K e^{\alpha t_0}, \end{aligned}$$

where $x_n = u_{k_n}(\mu^{-1}(\mu(s_n) + (k-n)t_0 - kt_0))$. Therefore, $Gv_n \rightarrow 0$ in $C_0(\mathbb{R}, E)$, and thus $0 \in A\sigma(G)$. This proves (7) and thus (6) holds. \square

Corollary 3.2. *The spectrum $\sigma(T_t)$ is rotationally invariant for $t > 0$, that is*

$$\lambda\sigma(T_t) = \sigma(T_t), \text{ for every } \lambda \in \mathbb{C} \text{ with } |\lambda| = 1. \quad (10)$$

Proof. For each $\gamma \in \mathbb{R}$ we define the isometry

$$\Psi_\gamma u(s) = e^{i\gamma\mu(s)}u(s), \quad u \in C_0(\mathbb{R}, E).$$

We have

$$\begin{aligned} \Psi_\gamma T_t \Psi_{-\gamma} u(s) &= e^{i\gamma\mu(s)}U(s, \mu^{-1}(\mu(s) - t))e^{-i\gamma(\mu(s) - t)}u(\mu^{-1}(\mu(s) - t)) \\ &= e^{i\gamma t}T_t u(s). \end{aligned}$$

It is well-known that the generator of the C_0 -semigroup $\{\Psi_\gamma T_t \Psi_{-\gamma}\}_{t \geq 0}$ is $\Psi_\gamma G \Psi_{-\gamma}$ and $\sigma(G) = \sigma(\Psi_\gamma G \Psi_{-\gamma})$ (see, for instance, [4, II.2.1]). On the other hand, the generator of $\{e^{i\gamma t}T_t\}_{t \geq 0}$ is $G + i\gamma I$ and $\sigma(G + i\gamma I) = \sigma(G) + i\gamma$ [4, II.2.1]. All these show that

$$\sigma(G) = \sigma(G) + i\gamma, \quad \gamma \in \mathbb{R}.$$

Finally, the spectral mapping theorem and the above identity prove (10). \square

Comments

Throughout this paper, all the results stand for $C_0(\mathbb{R}, E)$. Evidently they can be extended similarly to the general context of nonuniform behavior, formally replacing the function space $C_0(\mathbb{R}, E)$ with the super-space C_* introduced in [1]. However, such an approach would significantly complicate computations, without adding any essential merit for the main purpose.

References

- [1] L. Barreira, L. H. Popescu, C. Valls, *Nonuniform exponential behavior via evolution semigroups*, *Mathematika* 66 (2020), 15–38.
- [2] L. Barreira, C. Valls, *Growth rates and nonuniform hyperbolicity*, *Discrete Cont. Dyn. Syst.* 22 (2008), 509–528.
- [3] C. Chicone, Y. Latushkin, *Evolution Semigroups in Dynamical Systems and Differential Equations*, *Math. Surveys Monogr.* 70, Amer. Math. Soc. (1999).
- [4] K. J. Engel, R. Nagel, *One-Parameter Semigroups for Linear Evolution Equations*, *Grad. Texts in Math.* 194, Springer (2000).
- [5] N. Lupa, L. H. Popescu, *Generalized evolution semigroups and general dichotomies*, *Results Math.* 78 (2023): 112.
- [6] F. Rübiger, R. Schnaubelt, *The spectral mapping theorem for evolution semigroups on spaces of vector-valued functions*, *Semigroup Forum* 52 (1996), 225–239.

Nicolae Lupa – Department of Mathematics,
Politehnica University of Timișoara,
Piața Victoriei 2, 300006 Timișoara, Romania
E-mail: nicolae.lupa@upt.ro